CDF/PHYS/BOTTOM/CDFR/10264
Version 3.
July 14, 2011

Measurements of branching fractions and CP asymmetries in the Doubly Cabibbo Suppressed decay modes $B^{\pm} \to D^0 h^{\pm}$ on 7 fb^{-1}

P. Garosi[1], G. Punzi[2], P. Squillacioti[3]

Abstract

The branching fractions and CP asymmetries of $B^- \to D^0 K^-$ modes allow a theoretically-clean way of measuring the CKM angle γ. The "ADS method"[1][2] makes use of modes where the D^0 decays in a Doubly Cabibbo Suppressed (DCS): $D^0 \to K^+\pi^-$. This is a powerful method, but the corresponding decay has not yet been observed due to its rarity and the presence of large backgrounds.

Using a sample of about 7 fb^{-1} of data, we obtain evidence for the $B \to D^0_{DCS} K$ signal, at a level of 3.2σ, and we perform a measurement of the direct CP asymmetry for the DCS modes $B^{\pm} \to D^0\pi^{\pm}$ and $B^{\pm} \to D^0 K^{\pm}$.

We obtain, for the ADS parameters (definitions in the text):

$$R_{ADS}(\pi) = (2.8 \pm 0.7\ (stat.) \pm 0.4\ (syst.)) \cdot 10^{-3}$$

$$R_{ADS}(K) = (22.0 \pm 8.6\ (stat.) \pm 2.6\ (syst.)) \cdot 10^{-3}$$

$$A_{ADS}(\pi) = 0.13 \pm 0.25\ (stat.) \pm 0.02\ (syst.)$$

$$A_{ADS}(K) = -0.82 \pm 0.44\ (stat.) \pm 0.09\ (syst.)$$

$$R^+(\pi) = (2.4 \pm 1.0\ (stat.) \pm 0.4\ (syst.)) \cdot 10^{-3}$$

$$R^-(\pi) = (3.1 \pm 1.1\ (stat.) \pm 0.4\ (syst.)) \cdot 10^{-3}$$

$$R^+(K) = (42.6 \pm 13.7\ (stat.) \pm 2.8\ (syst.)) \cdot 10^{-3}$$

$$R^-(K) = (3.8 \pm 10.3\ (stat.) \pm 2.7\ (syst.)) \cdot 10^{-3}$$

[1]INFN Pisa, Siena University
[2]INFN Pisa, Pisa University
[3]Fermilab

1 Introduction

Several methods have been devised, based on the partial widths of $B \to D^0 K$ modes, to obtain a measurement of angle $\gamma = arg(-V_{ud}V_{ub}^*/V_{cd}V_{cb}^*)$:

- The GLW (Gronau-London-Wyler) method [3][4] uses $D^0_{flav} \to K^-\pi^+$, $D^0_{CP^+} \to K^+K^-, \pi^+\pi^-$ and $D^0_{CP-} \to K^0_s\pi^0, K^0_s\Phi, K^0_s\omega$.
- The ADS (Atwood-Dunietz,-Soni) method [1][2] uses $D^0_{flav} \to K^-\pi^+$ and the doubly cabibbo suppressed $D^0_{DCS} \to K^+\pi^-$.
- The Dalitz method [2][5] uses $D^0_{flav} \to K^0_s\pi^+\pi^-$.

All these methods require no tagging of the flavor or time-dependent measurements.

In this note we apply the ADS method. The ADS method exploits the interference between the $B^- \to D^0K^- \to [K^+\pi^-]K^-$ amplitude (color allowed $b \to c$ transition followed by the DCS D^0 decay) and the $B^- \to \overline{D}^0K^- \to [K^+\pi^-]K^-$ amplitude (color suppressed $b \to u$ transition followed by a Cabibbo allowed $\overline{D}^0$ decay). The observables needed for the γ measurement are:

- $R_{ADS} = \dfrac{BR(B^- \to [K^+\pi^-]_D K^-) + BR(B^+ \to [K^-\pi^+]_D K^+)}{BR(B^- \to [K^-\pi^+]_D K^-) + BR(B^+ \to [K^+\pi^-]_D K^+)}$
- $A_{ADS} = \dfrac{BR(B^- \to [K^+\pi^-]_D K^-) - BR(B^+ \to [K^-\pi^+]_D K^+)}{BR(B^- \to [K^+\pi^-]_D K^-) + BR(B^+ \to [K^-\pi^+]_D K^+)}$.

where D can be both D^0 or $\overline{D}^0$.
A_{ADS} and R_{ADS} are related to the angle γ, r_B, δ_B, the magnitude r_D of the ratio of the suppressed process $\overline{D}^0 \to K^-\pi^+$ over the favored $D^0 \to K^-\pi^+$, and the relative strong phase δ_D between these two amplitudes, through the relations:

$$R_{ADS} = r_D^2 + r_B^2 + 2r_D r_B \cos\gamma \cos\delta_B + \delta_D \quad (1)$$

$$A_{ADS} = 2r_B r_D \sin\gamma \sin\delta_B + \delta_D / R_{ADS} \quad (2)$$

The current status of experimental knowledge is [6]:

- Babar ($N(B\bar{B}) = 467$ M): $R_{ADS}(K) = 0.011 \pm 0.006 \pm 0.002$, $A_{ADS}(K) = -0.86 \pm 0.47^{+0.12}_{-0.16}$
- Belle ($N(B\bar{B}) = 772$ M): $R_{ADS}(K) = 0.0162 \pm 0.0042^{+0.0016}_{-0.0019}$, $A_{ADS}(K) = -0.39 \pm 0.26^{+0.06}_{-0.04}$

We measured also R_{ADS} and A_{ADS} also for the $B \to D^0\pi$ decay mode [6]. As can be seen from the expression (1), the maximum achievable value of the asymmetry is $A_{ADS}(max) = 2r_B r_D/(r_B^2 + r_D^2)$, where r_B can be $r_B(DK)$ or $r_B(D\pi)$. While r_D is known with a good precision ($r_D^2 = (3.80 \pm 0.18) \cdot 10^{-3}$) [17] and measurements on $r_B(DK)$ are

improving its resolution ($r_B(DK) = 0.103^{+0.015}_{-0.024}$) [7], there are no precise measurements for $r_B(D\pi)$. Looking at the Feynman diagrams, we expect that $r_B(D\pi)$ is suppressed by a factor $|V_{cd}V_{us}/V_{ud}V_{cs}| \sim \tan^2\theta_C$ with respect to $r_B(DK)$: we consider the same color suppression factor for both DK and $D\pi$ modes and θ_C the Cabibbo angle. For $r_B(DK) = 0.10$ and $r_B(D\pi) = 0.005$ we expect $A_{ADS}(max) \approx 0.90$ for the kaon and $A_{ADS}(max) \approx 0.16$ for the pion, both different from zero.
In [6] they estimate the order of magnitude $r_B(\pi) \sim 0.01$, for which $A_{ADS}(max) \approx 0.30$.

For the $B \to D^0\pi$ mode the current experimental status is:

- Babar ($N(B\bar{B}) = 467$ M): $R_{ADS}(\pi) = 0.0033 \pm 0.0006 \pm 0.0004$, $A_{ADS}(\pi) = 0.03 \pm 0.17 \pm 0.04$
- Belle ($N(B\bar{B}) = 772$ M): $R_{ADS}(\pi) = 0.00328 \pm 0.00037^{+0.00022}_{-0.00023}$, $A_{ADS}(\pi) = -0.04 \pm 0.11^{+0.01}_{-0.02}$

In this note we present the analysis of these modes using 5 fb^{-1}. We performed a simultaneous unbinned Maximum Likelihood fit of all modes mentioned above, combining mass and particle identification information. This is similar to the method used in the DCP analysis [8][9] and uses most of the same tools.

2 Data sample

To perform the analysis we need to reconstruct the following decays:

- CF: $B^- \to D^0_{CF}h^- \to [K^-\pi^+]_D\, h^- + c.c.$
- DCS: $B^- \to D^0_{DCS}h^- \to [K^+\pi^-]_D\, h^- + c.c$
- CS: $B^-_{CS} \to \overline{D}^0 h^- \to [K^+\pi^-]_D\, h^- + c.c.$

where CF is the Cabibbo Favored mode, h can be π or K, DCS means Doubly Cabibbo Suppressed and CS is Color Suppressed.
Experimentally there is no distinction between DCS and CS decays, as they decay exactly in the same final state. They make up a single sample that in the following we will call "DCS" for brevity.

Our data sample was collected by the B_CHARM trigger until July 2010, Period 0 to Period 31. We used the standard good run list following the prescription of the B-Group (Good Run list V37, goodrun_b_bs_nocal_nomu.list). The integrated luminosity of the sample is about 7 fb^{-1}. The offline version used is the 6.1.4 and the datasets used are: xbhdid, xbhdih, xbhdii, xbhdij, xbhdik, xbhdfm, xbhdfn and xbhdfp.

The candidates $B \to D^0\pi$ and $B \to D^0K$ are reconstructed from the B-DPi-KPi block of BStntuple.

The relevant cuts applied in this block are:

- minimum B mass = 4.40 GeV/c^2

- maximum B mass = 6.60 GeV/c^2
- minimum D^0 mass = 1.770 GeV/c^2
- maximum D^0 mass = 1.970 GeV/c^2
- maximum $\chi^2 = 25$
- set Mass Constraint
- Include Wrong Sign.

Each D^0 candidate is reconstructed with both possible $K\pi$ mass assignments. Only one candidate is kept in each case, based on the reconstructed masses (see next section), leading to two mutually exclusive samples "CF" and "DCS".

3 Cuts Optimization

Due to the smallness of the DCS Branching Ratio ($\sim 3.5 \cdot 10^{-3}$ times the CF Branching Ratio), the main issue for this analysis is the suppression of the backgrounds.

3.1 Basic requirements

The cuts optimization has been performed on 5 fb^{-1}. In Fig. 1 we can see the distribution of the B candidate masses for the two samples, after the preliminary cuts listed below. A $B \to D^0\pi$ CF signal is visible, while the DCS signal appears to be buried in the combinatorial background.

- B decay length significance: $\dfrac{L_{xy}(B)}{\sigma_{L_{xy}(B)}} \geq 8$;
- B decay length error: $\sigma_{L_{xy}(B)} \leq 0.01$;
- B impact parameter: $|d_0(B)| \leq 0.008$ cm;
- B transverse momentum: $p_t(B) \geq 5$ GeV/c^2;
- D decay length measured with respect to the B decay vertex: $L_{xy}(D)_B \geq -0.015$ cm;
- $\Delta R = \sqrt{\Delta\Phi^2 + \Delta\eta^2}$ between the track from B and the D^0: $\Delta R \leq 2$;
- Eta of the track from B: $|\eta| \leq 1.$;
- Eta of the tracks from D: $|\eta| \leq 1.$;
- transverse momentum of the track from B: $p_t \geq 1$ GeV/c^2;

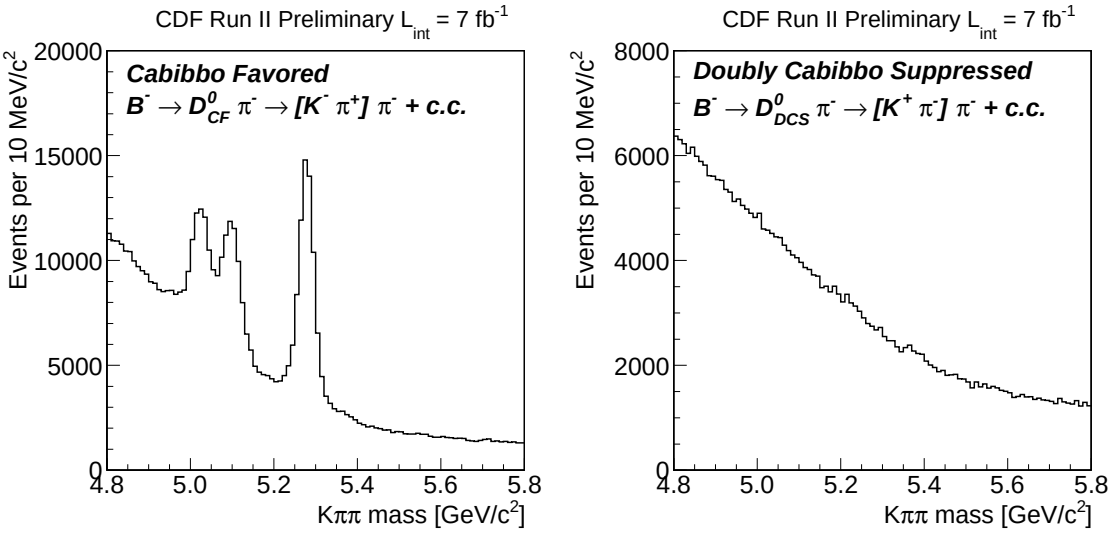

Figure 1: Invariant mass distribution of $B^- \to D^0\pi^-$ CF on the left and DCS on the right after preliminary cuts.

We also apply three cuts (one of selection + two vetos) to the D^0 mass. We apply cuts symmetrically to both CF and DCS samples to ensure equal selection efficiency. Indeed, the strict similarity between CF and DCS signals is a strong point of this analysis.

- the final cut value for the D^0 mass is obtained in the optimization procedure 3.2
- veto cut of 4σ on Wrong Sign (WS) D^0 mass assignment:
  $M(D^0_{WS}) \leq 1.8245,\ M(D^0_{WS}) \geq 1.9045$.
  If the correct mass assumption (RS) to the tracks forming a D^0 is $K\pi$, we calculated, for each event, also the invariant mass in the assumption of πK (WS). In Fig. 2 is shown the distribution of the correct mass assignment (y-axis) vs the wrong sign (x-axis) for DCS. The veto cuts a slice in the x-axis removing the events that can have both right sign and wrong sign assignment.

- veto cut of 4σ on the D^0 invariant mass constructed with one track from D^0 and the track from B:
  $M(D^0_{K\pi_B}) \leq 1.8245,\ M(D^0_{K\pi_B}) \geq 1.9045$.
  This cut insure that CF events passing the DCS selection, in which the invariant mass constructed with a track from B and the kaon from D^0 is peaked on D^0 mass, are removed. The vice versa is also applied.

To have a good agreement between MC and data we applied offline trigger cuts, requiring the confirmation of "Scenario A" for one of the two tracks from D^0 and the track from B. These cuts have the only aim to remove "volunteers" tracks from data, that are not simulated in MC.

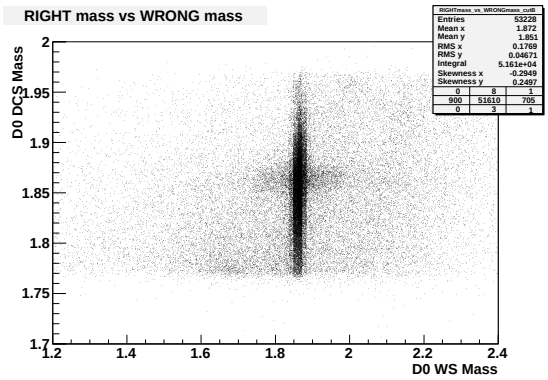

Figure 2: Invariant mass distribution of D^0 candidate in the $K\pi$ hypothesis vs πK hypothesis (wrong-sign).

3.2 Details on cuts optimization

The cuts optimization is focused on finding an evidence for $B \to D^0_{DCS}\pi$ mode. Since the sample $B \to D^0_{CF}\pi$ has the same topology of the DCS one, we performed the cuts optimization on CF mode.
We chose the $B \to D^0\pi$ signal region between $\pm 2\sigma$ around B mass ($5.243\ \text{GeV}/c^2 \leq M(B) \leq 5.315\ \text{GeV}/c^2$), sideband subtracted, and, as background region, the mass window $5.4\ \text{GeV}/c^2 \leq M(B) \leq 5.8\ \text{GeV}/c^2$, where only combinatorial background and no physics background appears.

We maximized the figure of merit $\dfrac{S}{1.5+\sqrt{B}}$ [10], where S is the signal and B the background number of events.
The variables used for the optimization are:

- D^0 Mass: $M(D)$;
- B decay length significance: $\dfrac{L_{xy}(B)}{\sigma_{L_{xy}(B)}}$;
- B impact parameter: $|d_0(B)|$
- B tridimensional vertex quality: $\chi^2_{3D}(B)$
- ΔR between the track from B and the D^0
- B Isolation (Cone of Radius 1): $Isol_1$;
- B Isolation (Cone of Radius 0.4): $Isol_{0.4}$;
- B pointing angle: $PA(B)$;
- D angular distribution: $\cos\theta^*_D$;
- Difference $\kappa(K_D) - \kappa(\pi_D)$.

All these variables have a different distribution for signal and background, so they can distinguish signal from background. Figs. 3 and 4 show the distributions for all variables: in black for signal events (sideband subtracted) and in red for the background.

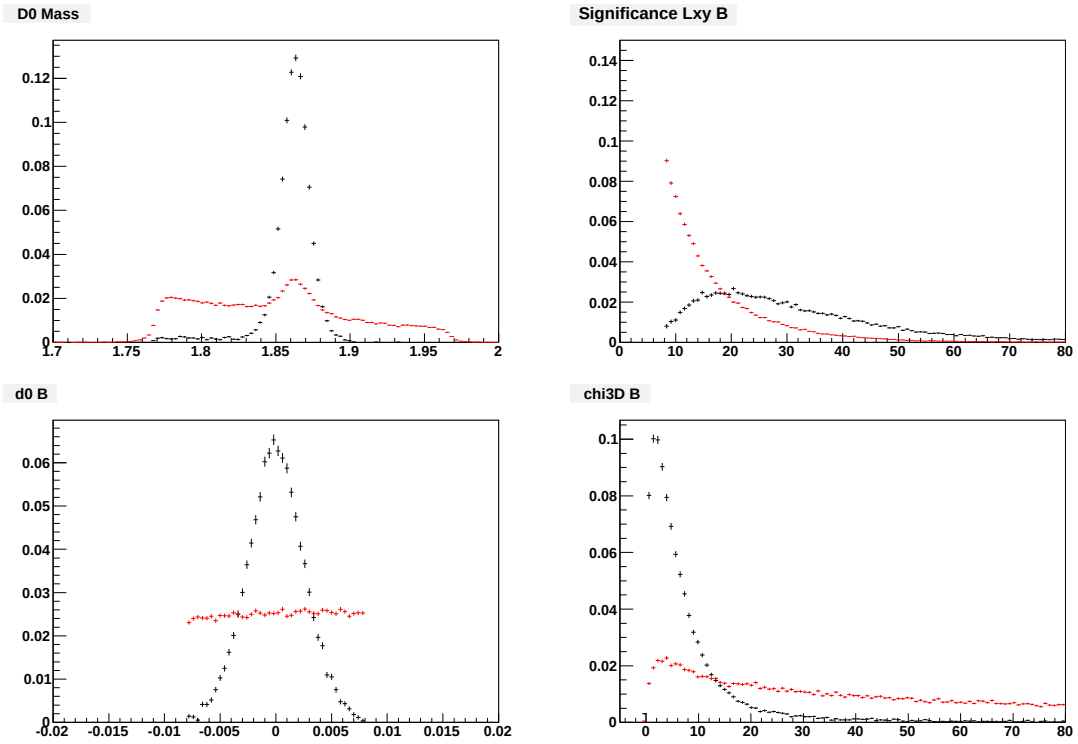

Figure 3: From left to right we have the distribution of variables D^0 *Mass*, $\frac{L_{xy}(B)}{\sigma_{L_{xy}(B)}}$, $|d_0(B)|$ and $\chi^2_{3D}(B)$ in the signal region (in black) and in the background region (in red).

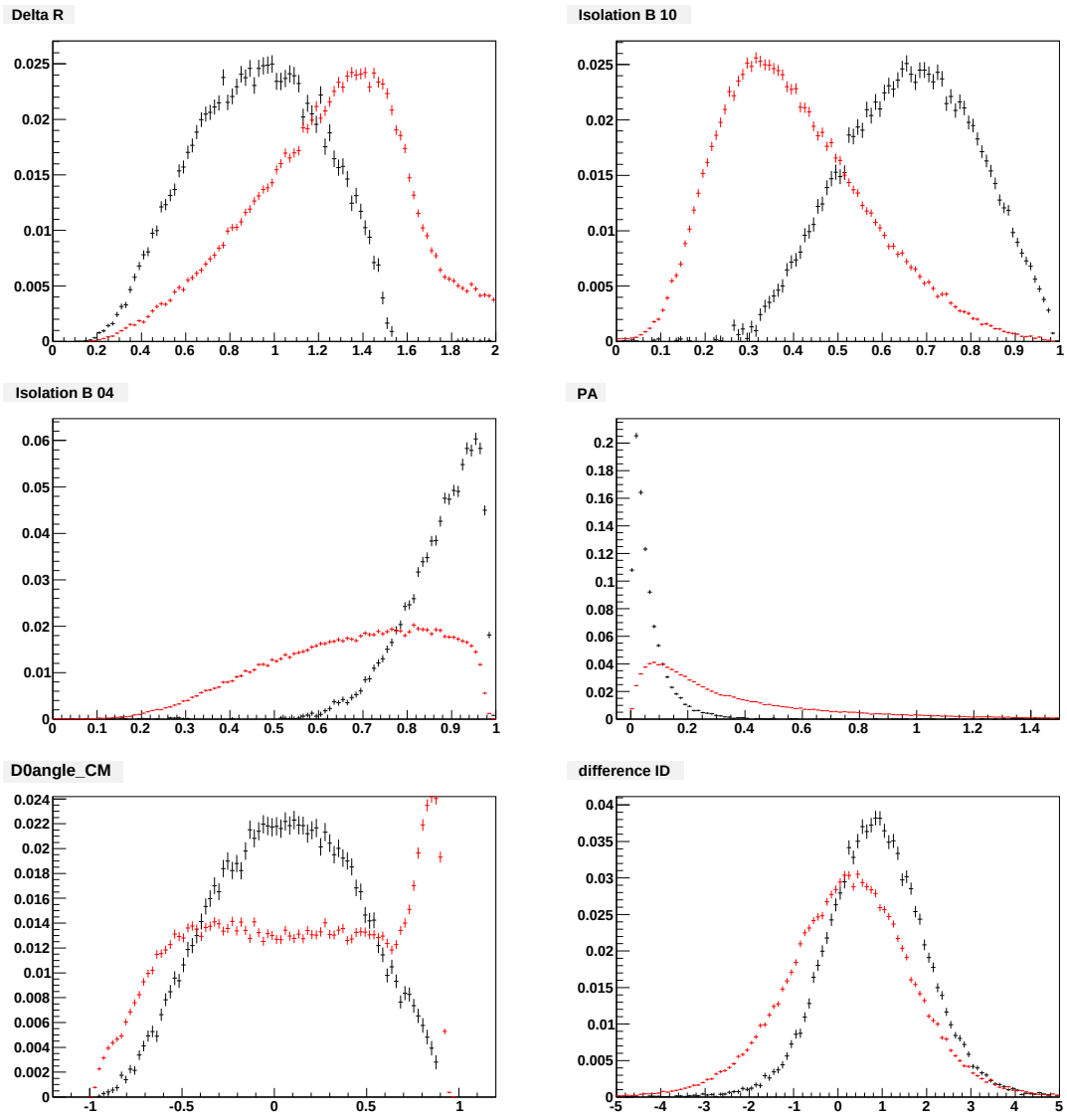

Figure 4: From left to right we have the distribution of variables ΔR , $Isol_1$, $Isol_{0.4}$, $PA(B)$, $\cos\theta_D^*$ and $\kappa(K_D) - \kappa(\pi_D)$ in the signal region (in black) and in the background region (in red).

The two *Isolations* at radius 1. and 0.4 have a small correlation and together can remove better the background than using only one of them.
The *Pointing Angle* is defined as the angle between the 3-dimensional momentum of B and the 3-dimensional decay lenght. Signal events will have small pointing angles, while background events will have bigger angles.
The *angular distribution of* D^0 is defined as the cosine of the angle between the D^0 in the Center of Mass (CM) of the B, and the flight direction of B.
The variable $\kappa(i)$, called *kaoness*, is defined as $\kappa(i) = \dfrac{dE/dx_{meas}(i) - dE/dx_{exp}(\pi)}{dE/dx_{exp}(K) - dE/dx_{exp}(\pi)}$, where $i = K, \pi$ from D^0. The kaoness is centered in 0 if the track is a pion and in 1 if it is a kaon. We verified that the *difference* has a greater power separation than using single κ.

The cuts selection that maximize the figure of merit is the following:

- D^0 mass: $M(D) \leq 1.8645 + 1.5 \times 0.01$ and $M(D) \leq 1.8645 - 1.5 \times 0.01$;
- B decay length significance: $\dfrac{L_{xy}(B)}{\sigma_{L_{xy}(B)}} \geq 12$;
- B impact parameter: $|d_0(B)| \leq 0.005$ cm;
- B tridimensional vertex quality: $\chi_{3D} \leq 13$;
- $\Delta R = \sqrt{\Delta\Phi^2 + \Delta\eta^2}$ between the track from B and the D^0: $\Delta R \leq 1.5$;
- B Isolation (Cone 1): $Isol \geq 0.4$;
- B Isolation (Cone 0.4): $Isol \geq 0.7$;
- B pointing angle: $PA(B) \leq 0.15$;
- D angular distribution: $|\cos(\theta^*_D)| \leq 0.6$;
- Difference $\kappa(K_D) - \kappa(\pi_D) \geq -1$.

We added also a cut on the D^0 decay length measured with respect to the B decay vertex ($Lxy(D)_B$).
This cut is not included in the optimization procedure, since it is chosen to suppress the physics background B to three body decay. As can be seen in Fig. 5, three body decays (red curve) have a smaller $Lxy(D)_B$ than charm B decays (black curve).

Adding the cut:

- $Lxy(D)_B \geq 0.01$

we verified from MC that 3-body backgrounds are removed of about 75% and signal of about 20%.

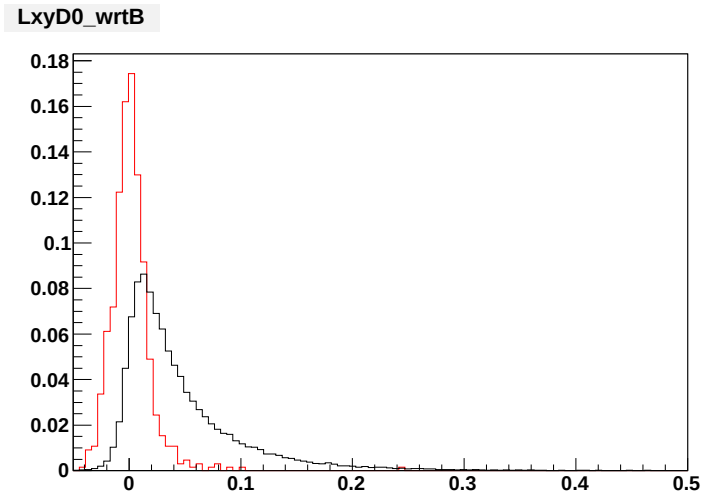

Figure 5: Distribution of $Lxy(D)_B$ of a three body decay (red curve) and a charm B decay (black curve).

The resulting invariant mass distributions, with pion mass assignment to the track from B, were reported in Fig. 6, the invariant mass distribution of $B^- \to D^0\pi^- \to [K^-\pi^+]_D\pi^-$ (CF) and $B^- \to D^0\pi^- \to [K^+\pi^-]_D\pi^-$ (DCS).

We can see that the combinatorial background is almost reduced to zero, as was our aim.

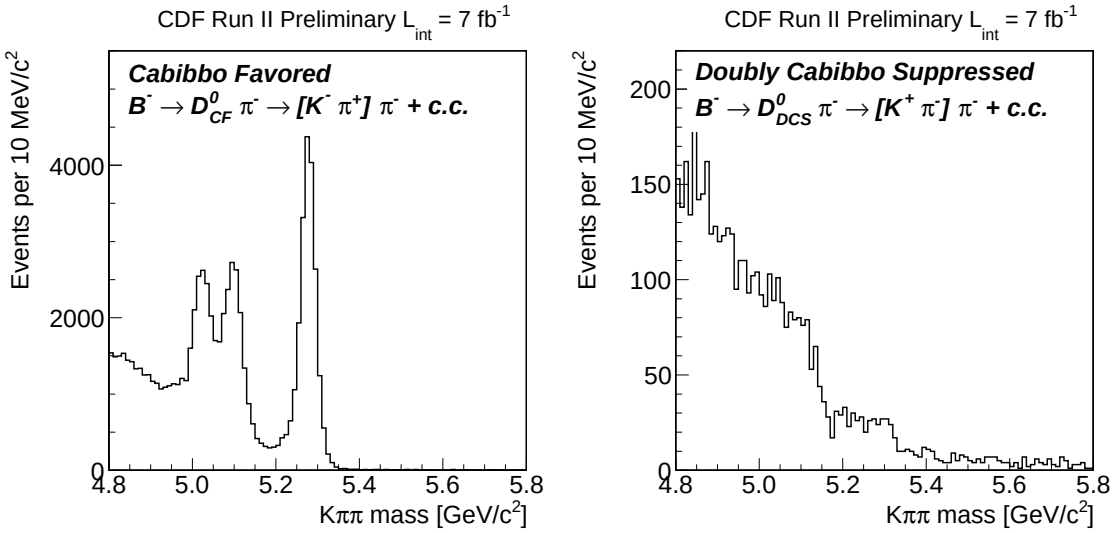

Figure 6: Invariant mass distribution of $B^- \to D^0\pi^-$ CF on the left and DCS on the right after optimized cuts.

4 MC simulation

Monte Carlo sample of $B^- \to D^0 h^-$ has been generated with final state radiation (loss of energy from soft photon emission from the charged final state particles) modeled with PHOTOS as implemented in EvtGen. We used the standard B-Monte Carlo release, patch r, good run list named 6.1.4
We observed a discrepancy between the $p_t(B)$ distributions of the simulated B candidates and of B candidates reconstructed on real data (Fig. 7). We selected the signal region in a window of plus/minos 2σ around the B peak, sideband subtracted. For the sideband subtraction, after defining the background region in the window [5.4,5.8] GeV/c^2, we normalized the background to the signal region and we subtracted the events. We reweighted the MC $p_t(B)$ distribution in order to obtain a better agreement between data and simulation. We fit with an Erfc function plus a first degree polynomial (shown in Fig. 8) the distribution of the data/MC ratio and we reweigthed the $p_t(B)$ distribution of the simulated events accordingly. The agreement between MC and data after the reweighting is satisfactory (Figs. 9-14). In all the Figs. we show data as points with error bars and MC as lines.

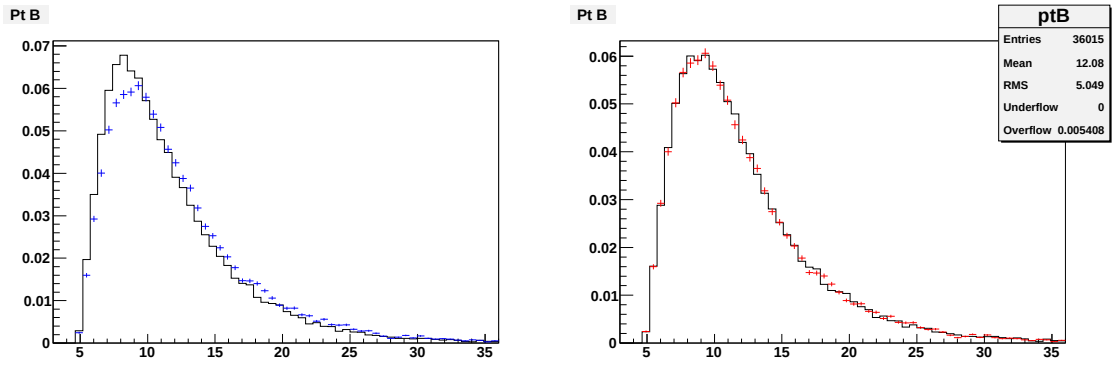

Figure 7: Data (points) - simulation (line) comparison of the $p_t(B)$ distribution. Left plot: $p_t(B)$ distributions before the reweighting. Right plot: $p_t(B)$ distributions after the reweighting.

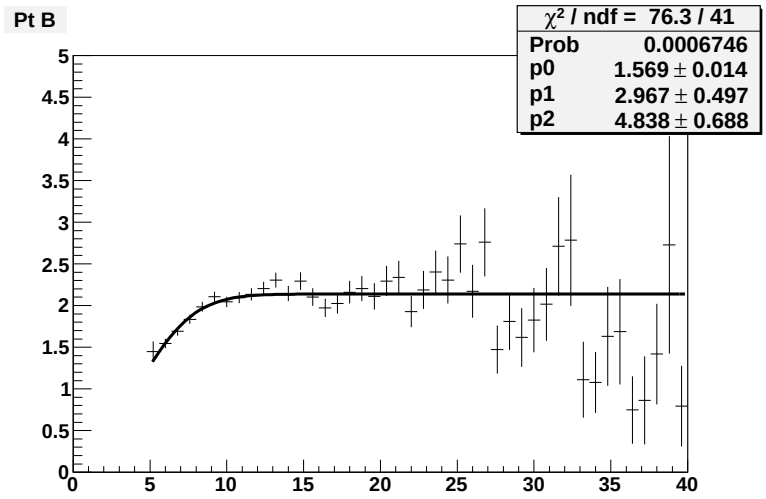

Figure 8: Distribution of the data(points)/MC(line) ratio fitted with an Erfc function plus a first degree polynomial.

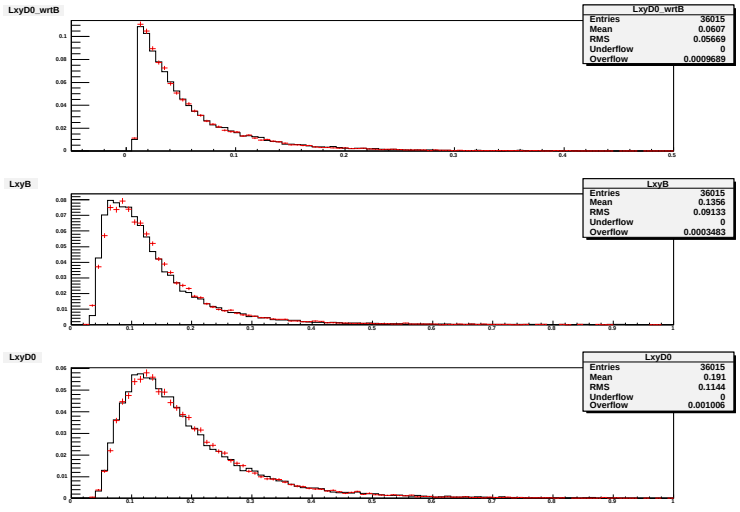

Figure 9: Top: D decay lenght measured with respect to the B deacy vertex. Middle: B decay lenght. Bottom: D decay lenght.

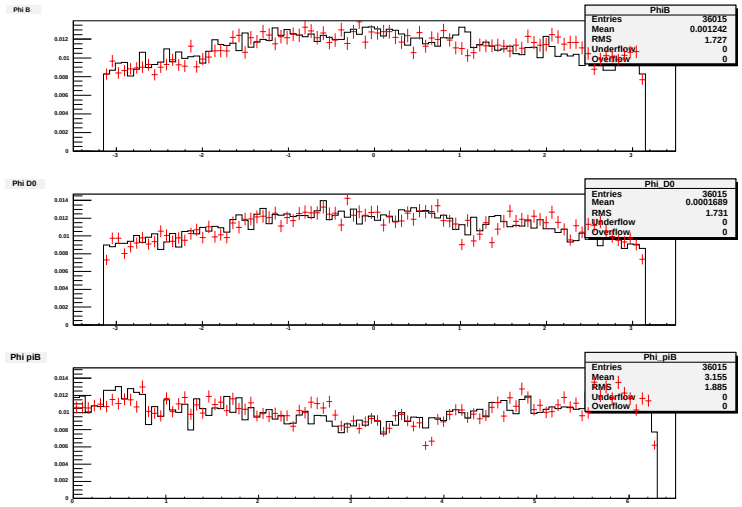

Figure 10: Top: Phi of B. Middle: Phi of D^0. Bottom: Phi of the pion from B.

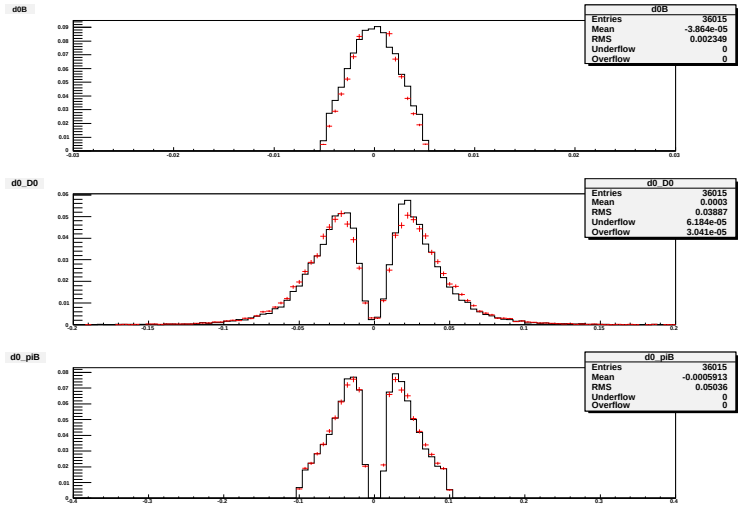

Figure 11: Top: B impact parameter. Middle: D^0 impact parameter. Bottom: Impact parameter of the pion from B.

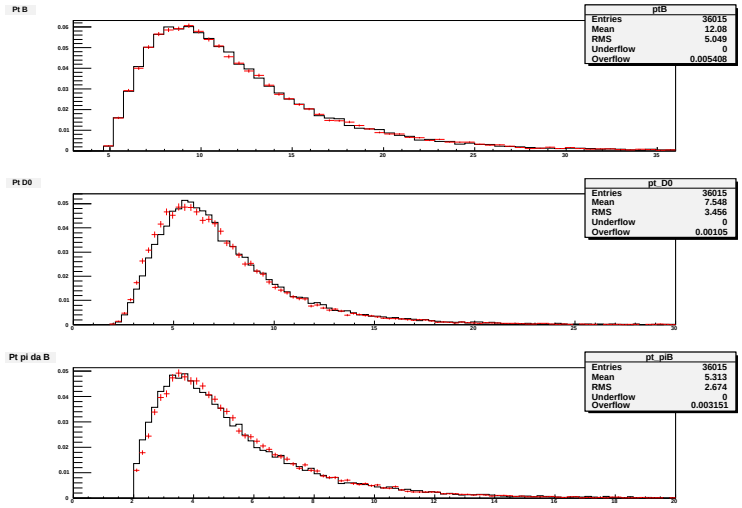

Figure 12: Top: $p_t(B)$. Middle: $p_t(D^0)$. Bottom: p_t(pion from B)

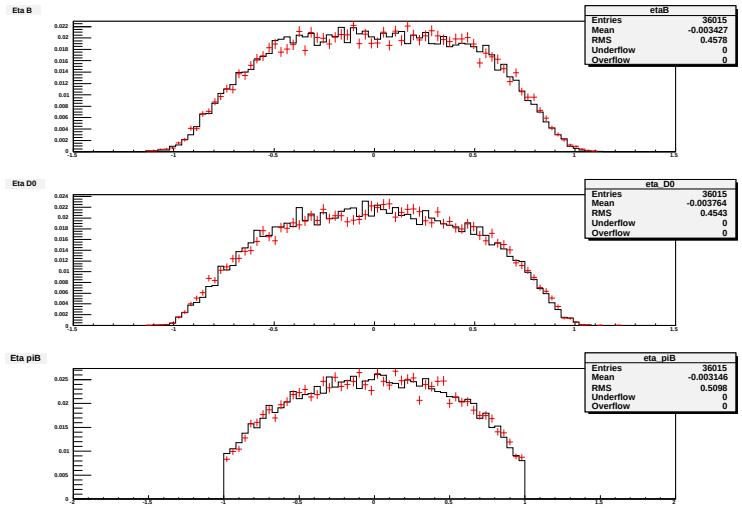

Figure 13: Top: Eta of B. Middle: Eta of D^0. Bottom: Eta of the pion from B.

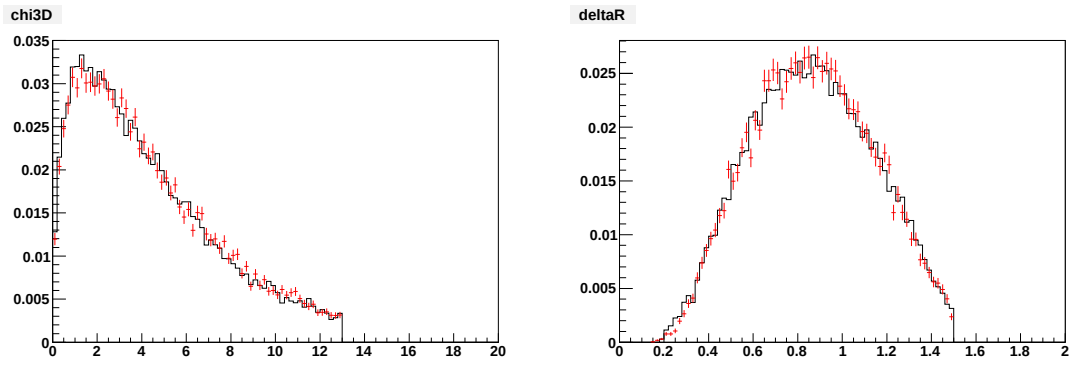

Figure 14: Left: tridimensional χ^2. Right: $\Delta R = \sqrt{\Delta\Phi^2 + \Delta\eta^2}$ between the track from B and the D^0.

5 Fit range

We are performing a fit using the information of mass shapes and particle identification (PID). For the mass we chose the range between 5.17 and 6.5 GeV/c^2. As in the DCP analysis [8][9], we chose the lower limit 5.17 since the only other mode significantly contributing to the $B \to DK$ mass region is the $B^+ \to \overline{D}^{0*}\pi^+$. We extend the fit up to 6.5 because the combinatorial background with the optimized cuts is very low and we need to have a major lever to take into the right way the slope and the fraction of the combinatorial background.

For what concern particle identification we fit PID variable (see Sec. 9) in the region [-3,+3].

6 Background study for the DCS mode

There are several physics backgrounds that appear in the DCS reconstruction. We will consider each category.

6.1 $B \to D^0\pi$ with $D^0 \to X$

The CF mode itself is a source of background for the DCS. We checked from MC that CF events in which the D^0 radiate a photon in the final state, if reconstructed as DCS, can skip the WS veto cut. We estimate a fraction of these events, with respect to the $B \to D^0\pi$ (CF) to be about $1.4 \cdot 10^{-3}$. Since the $B \to D^0\pi$ DCS branching fraction with respect to CF is about $3.5 \cdot 10^{-3}$ this background is significant.

We found many other decays that behave as background for the DCS, such as $B \to D^0\pi$, with $D^0 \to \pi^-\mu^+\nu_\mu$, $D^0 \to K^-\pi^+\pi^0$, $D^0 \to \rho^-\pi^+$, $D^0 \to \rho^+\pi^-$.

We decided to consider all decays together as a single background, generating a MC sample of $B \to D^0\pi$ with $D^0 \to X$, with official relative BRs, that we report also in Appendix A. After removing $B^- \to D^0\pi^- \to [K^+\pi^-]_D\pi^-$ in the reconstruction we evaluated the remaining background fraction, with respect to $B \to D^0\pi$ CF, of about $5.1 \cdot 10^{-3}$, which corresponds to about 100 events in the mass fit window.
Considering all backgrounds together will produce a better resolution in the final fit, since we will fit only the normalization, while all contributions are each other fixed to the relative BRs.

6.2 $B \to D^0K$ with $D^0 \to X$

As for the previous case we generated a MC sample of $B \to D^0K$ with $D^0 \to X$ with relative D^0 BRs as in Appendix A. After removing $B^- \to D^0K^- \to [K^+\pi^-]_DK^-$ in the reconstruction, we evaluated a fraction of background, over the $B \to D^0K$ CF, of about $2.3 \cdot 10^{-3}$, which corresponds to about 5 events in the mass fit window.

6.3 $B \to D_{CP}^{0(*)} h$ with $D^0 \to K^+K^-, \pi^+\pi^-$

We verified using MC samples that none of $B \to D_{CP}^{0(*)} h$ modes, where $D^{0(*)}$ can be D^0 or D^{0*}, reconstructed as DCS, appear as background. The only "dangerous" could be $B \to D^0 K$ with $D^0 \to \pi^+\pi^-$, but, after all the cuts and normalizing for the BR, its contribution is negligible.

6.4 B^- to three-body decays

The only two 3-body decays that can affect our measurement are $B^- \to K^+\pi^-K^-$, peaking in the $B \to D^0 K$ mass region, and $B^- \to K^+\pi^-\pi^-$, peaking in the $B \to D^0\pi$ mass region.
The first one is negligible after the cut on $L_{xy}(D)_B$. The second one has a fraction of events with respect to $B \to D^0\pi$ CF of about $5.5 \cdot 10^{-4}$, which corresponds to about 11 events in the mass fit window. It has been added to the fit.

6.5 $B^0 \to D_0^{*-} e^+ \nu_e$

We generated MC samples of $B^0 \to D_0^{*-} e^+ \nu_e$ and we evaluated a fraction with respect to $B \to D^0\pi$ CF of about $2.4 \cdot 10^{-4}$, corresponding to about 5 events in the mass window.

6.6 Other decays

We generated MC samples of $B_s \to D_s^- \pi^+$, with $D_s^- \to X$, $B^0 \to D^-\pi^+$, with $D^- \to X$, $B^- \to D^0\rho^-$ with $D^0 \to K^-\pi^+$, $B^- \to D^0\mu^-\nu_\mu$ with $D^0 \to K^-\pi^+$, $B^- \to D^0 e^-\nu_e$ with $D^0 \to K^-\pi^+$, $B^- \to D^{*0}K^-$ with $D^0 \to K^-\pi^+$, $B^- \to D^{*0}\mu^-\nu_\mu$ with $D^0 \to K^-\pi^+$, $B^- \to K^+\pi^-K^-$ and we found that all of them does not appear in the DCS reconstruction or give a negligible effect.

In conclusion the four backgrounds that we are going to consider for the DCS are: $B \to D^0\pi$ with $D^0 \to X$, $B \to D^0 K$ with $D^0 \to X$, $B^- \to K^-\pi^+\pi^-$ and $B^0 \to D_0^{*-} e^+\nu_e$. We applied a Gaussian constraint to the fit Likelihood to bind the fractions of these backgrounds. We chose as sigma of the constraint the sum in quadrature of the error propagated from the PDG BRs and the relative error coming from the MC statistics. In this way we include in the statistical error the error due to MC statistics.

- $N_{expected}(B \to D^0\pi,\, D^0 \to X / B \to D^0\pi) = 100$
  Sigma in the constraint = 3% (PDG) + 5.9% (coming from 290 reconstructed events in the final state) = 6.5%.
- $N_{expected}(B \to D^0 K,\, D^0 \to X) = 5$
  Sigma in the constraint = 9% (PDG) + 22% (coming from 20 reconstructed events in the final state) = 24%.
- $N_{expected}(B \to K^-\pi^+\pi^-) = 11$
  Sigma in the constraint = 6.6% (PDG) + 5.5% (coming from 333 reconstructed events in the final state) = 8.6%.

- $N_{expected}(B^0 \to D_0^{*-} e^+ \nu_e) = 5$
  Sigma in the constraint = 40% (PDG) + 14% (coming from 54 reconstructed events in the final state) = 42%.

7 Simultaneous Fit of $B \to D\pi$ and DK modes

We implemented an extended maximum Likelihood fit that combines the invariant mass ($M_{K\pi\pi}$) and the particle identification information.

We perform a simultaneous fit on CF mode and DCS modes. The expression of the non extended Likelihood is:

$$\mathcal{L}_{n.e.} = \mathcal{L}_{CF+} \cdot \mathcal{L}_{CF-} \cdot \mathcal{L}_{DCS+} \cdot \mathcal{L}_{DCS-}. \tag{3}$$

We multiply each factor for a Poisson distribution, with each expected mean values equal to the number of events on each sub-samples.

$$\mathcal{L} = \mathcal{P}_{CF+} \cdot \mathcal{L}_{CF+} \cdot \mathcal{P}_{CF-} \cdot \mathcal{L}_{CF-} \cdot \mathcal{P}_{DCS+} \cdot \mathcal{L}_{DCS+} \cdot \mathcal{P}_{DCS-} \cdot \mathcal{L}_{DCS-}. \tag{4}$$

The product of the four independent Poisson distributions is equivalent to take the product of a Poisson distribution, with expected mean values equal to the total number of events, multiplied by a multinomial distribution, which take into account the subdivision into the four sub-samples (cap 6.9 and 6.10 of [14]). Using an extended fit we ensure that errors take into account all correlations between fitted numbers of events and fitted fractions.

The single components are defined as:

$$\mathcal{P}_i = \frac{\mu^{N_i}}{N_i!} e^{-\mu}$$

$$\begin{aligned}
\mathcal{L}_{CF+} &= \prod_i^{N_{TOT}^{CF+}} \Big[(1 - b_{CF+}) \cdot \Big(f_\pi^{CF+} \cdot pdf_\pi(M,\kappa) + \mathbf{c}^+ \cdot f_\pi^{CF+} \cdot pdf_{D*}(M,\kappa) + \\
&\quad + \Big(1 - f_\pi^{CF+} - \mathbf{c}^+ \cdot f_\pi^{CF+} \Big) \cdot pdf_K(M,\kappa) \Big) + b_{CF+} \cdot pdf_{comb}(M,\kappa) \Big]
\end{aligned}$$

$$\begin{aligned}
\mathcal{L}_{CF-} &= \prod_i^{N_{TOT}^{CF-}} \Big[(1 - b_{CF-}) \cdot \Big(f_\pi^{CF-} \cdot pdf_\pi(M,\kappa) + \mathbf{c}^- \cdot f_\pi^{CF-} \cdot pdf_{D*}(M,\kappa) + \\
&\quad + \Big(1 - f_\pi^{CF-} - \mathbf{c}^- \cdot f_\pi^{CF-} \Big) \cdot pdf_K(M,\kappa) \Big) + b_{CF-} \cdot pdf_{comb}(M,\kappa) \Big]
\end{aligned}$$

$$\mathcal{L}_{DCS+} = \prod_i^{N_{TOT}^{DCS+}} \Big[(1 - b_{DCS+}) \cdot \Big(f_\pi^{DCS+} \cdot pdf_\pi(M,\kappa) + \mathbf{c}^+ \cdot f_\pi^{DCS+} \cdot pdf_{D*}(M,\kappa) +$$

$$+\left(1-f_\pi^{DCS+}-\mathbf{c}^+\cdot f_\pi^{DCS+}\right)\cdot pdf_K(M,\kappa)\Big)+$$
$$+b_{DCS+}\cdot\Big(f^+_{[X]\pi}\cdot pdf_{[X]\pi}(M,\kappa)+f^+_{[X]K}\cdot pdf_{[X]K}+f^+_{K\pi\pi}\cdot pdf_{K\pi\pi}(M,\kappa)+$$
$$f^+_{B^0}\cdot pdf_{B^0}(M,\kappa)+(1-f^+_{[X]\pi}-f^+_{[X]K}-f^+_{K\pi\pi}-f^+_{B^0})\cdot pdf_{comb}(M,\kappa)\Big)\Big]$$

$$\mathcal{L}_{DCS-} = \prod_i^{N_{TOT}^{DCS-}}\Big[(1-b_{DCS-})\cdot\Big(f_\pi^{DCS-}\cdot pdf_\pi(M,\kappa)+\mathbf{c}^-\cdot f_\pi^{DCS-}\cdot pdf_{D*}(M,\kappa)+$$
$$+\left(1-f_\pi^{DCS-}-\mathbf{c}^-\cdot f_\pi^{DCS-}\right)\cdot pdf_K(M,\kappa)\Big)+$$
$$+b_{DCS-}\cdot\Big(f^-_{[X]\pi}\cdot pdf_{[X]\pi}(M,\kappa)+f^-_{[X]K}\cdot pdf_{[X]K}+f^-_{K\pi\pi}\cdot pdf_{K\pi\pi}(M,\kappa)+$$
$$f^-_{B^0}\cdot pdf_{B^0}(M,\kappa)+(1-f^-_{[X]\pi}-f^-_{[X]K}-f^-_{K\pi\pi}-f^-_{B^0})\cdot pdf_{comb}(M,\kappa)\Big)\Big]$$

The parameters b_{CF+}, b_{CF-}, b_{DCS+} and b_{DCS-} are the fractions of the background for each mode and charge. In the CF likelihood the only background considered is the combinatorial, for which we use a single pdf_{comb} for both positive and negative charges. For the DCS we are considering the combinatorial (with the same pdf of CF mode) and the physical background, as $B\to K\pi\pi$ in three-body decay (of which the fraction is $f^\pm_{K\pi\pi}$ and $pdf_{K\pi\pi}$), $B\to D^0\pi$ with $D^0\to X$ (of which the fraction is $f^\pm_{[X]\pi}$ and $pdf_{[X]\pi}$), $B\to D^0K$ with $D^0\to X$ (of which the fraction is $f^\pm_{[X]K}$ and $pdf_{[X]K}$), and $B^0\to D_0^{*-}e^+\nu_e$ (of which the fraction is $f^\pm_{B^0}$ and pdf_{B^0}).

For the signals, $f_\pi^{CF,DCS,\pm}$ is the fraction of $B\to D^0\pi$ CF, DCS, positive and negative charges, $\mathbf{c}^\pm$ is the common parameter for CF and DCS likelihood and corresponds to the ratio of the $B\to D^*\pi$ over $B\to D^0\pi$. We verified from MC that for CF and D_{CP} modes this fraction remains constant and we are using it also for the DCS. The simultaneous fit allows us to take advantage of the CF channel with more statistics to constrain the common parameter $\mathbf{c}$ in a consistent way.

The fraction of $B\to D^0K$ is written as $(1-f_\pi-c\cdot f_\pi)$, so it is not explicitly fitted, but is calculated from the fraction of $B\to D^0\pi$ and $B\to D^{*0}\pi$. In this way, when we had to fix that fraction to zero, to evaluate the $B\to D^0K$ DCS significance, the fit found problems of convergence to realistic values. For this reason we decided to apply this change of variables in the DCS part of the likelihood:

$$\begin{aligned}1-f_\pi^{DCS}-\mathbf{c}\cdot f_\pi^{DCS} &= f_K^{DCS}\\ f_\pi^{DCS} &= 1-f_K^{DCS}-\mathbf{c}\cdot f_\pi^{DCS},\end{aligned}$$

where the second expression can be simplified in: $f_\pi^{DCS}=(1-f_K^{DCS})/(1+\mathbf{c})$.

In this way the formal expressions of the DCS likelihood are:

$$\mathcal{L}_{DCS+} = \prod_i^{N_{TOT}^{DCS+}}\Big[(1-b_{DCS+})\cdot\Big((1-f_K^{DCS+})/(1+\mathbf{c}^+)\cdot pdf_\pi(M,\kappa)+$$

$$
\begin{aligned}
&+\mathbf{c}^{+} f_{\pi}^{DCS+} \cdot pdf_{D*}(M,\kappa) + f_{K}^{DCS+} \cdot pdf_{K}(M,\kappa)\Big) + \\
&+b_{DCS+} \cdot \Big(f^{+}_{[X]\pi} \cdot pdf_{[X]\pi}(M,\kappa) + f^{+}_{[X]K} \cdot pdf_{[X]K} + f^{+}_{K\pi\pi} \cdot pdf_{K\pi\pi}(M,\kappa) + \\
&f^{+}_{B^0} \cdot pdf_{B^0}(M,\kappa) + (1 - f^{+}_{[X]\pi} - f^{+}_{[X]K} - f^{+}_{K\pi\pi} - f^{+}_{B^0}) \cdot pdf_{comb}(M,\kappa)\Big)\Big]
\end{aligned}
$$

$$
\begin{aligned}
\mathcal{L}_{DCS-} \;=\; \prod_{i}^{N_{TOT}^{DCS-}} &\Big[(1 - b_{DCS-}) \cdot \Big((1 - f_{K}^{DCS-})/(1 + \mathbf{c}^{-}) \cdot pdf_{\pi}(M,\kappa) + \\
&+\mathbf{c}^{-} f_{\pi}^{DCS-} \cdot pdf_{D*}(M,\kappa) + f_{K}^{DCS-} \cdot pdf_{K}(M,\kappa)\Big) + \\
&+b_{DCS-} \cdot \Big(f^{-}_{[X]\pi} \cdot pdf_{[X]\pi}(M,\kappa) + f^{-}_{[X]K} \cdot pdf_{[X]K} + f^{-}_{K\pi\pi} \cdot pdf_{K\pi\pi}(M,\kappa) + \\
&f^{-}_{B^0} \cdot pdf_{B^0}(M,\kappa) + (1 - f^{-}_{[X]\pi} - f^{-}_{[X]K} - f^{-}_{K\pi\pi} - f^{-}_{B^0}) \cdot pdf_{comb}(M,\kappa)\Big)\Big]
\end{aligned}
$$

The likelihood is the same as before, as a cross-check we verified that all yields and observables results remain the same, but the fraction of $B \to DK$ can be now directly fixed to zero allowing an easier evaluation of the significance. This is chosen as the final fit configuration.

pdf functions are functions of the Mass (M) in $[K\pi]\pi$ hypothesis and of Particle Identification (the κ kaoness variable applied to the track from B, defined in 3.2). They are different for each decay, but equal for CF and DCS Likelihoods.

In the next sections we will consider piece by piece all *pdf*s, and describe the parameterizations used for mass and Particle Identification variables.

8 Mass templates

8.1 Signal mass template

Monte Carlo samples of $B^- \to D^0\pi^-$ and of $B^- \to D^0K^-$ have been generated with final state radiation modeled with PHOTOS as implemented in EvtGen.

The mass line shape is parameterized using the following asymmetric pdf:

$$
\begin{aligned}
pdf(m;\vec{\theta}) = f_{fsr} \cdot &\left(\frac{1}{norm} \cdot e^{b_{fsr}\cdot(m-(mu+\Delta))} \cdot erfc(c_{fsr} \cdot (m - (mu + \Delta)))\right) \\
+ (1 - f_{fsr}) \cdot &\left(f_1 \frac{1}{\sigma_1 \cdot s \cdot \sqrt{2\pi}} e^{-\frac{1}{2}\left(\frac{m-(mu+\Delta)}{\sigma_1 \cdot s}\right)^2} + f_2 \frac{1}{\sigma_2 \cdot s \cdot \sqrt{2\pi}} e^{-\frac{1}{2}\left(\frac{m-(mu+\Delta)}{\sigma_2 \cdot s}\right)^2}\right. \\
+ &\left. f_3 \frac{1}{\sigma_3 \cdot \sqrt{2\pi}} e^{-\frac{1}{2}\left(\frac{m-(mu+\Delta)}{\sigma_3}\right)^2}\right)
\end{aligned}
\tag{5}
$$

where f_{fsr} is the contribution of the radiative tail fraction. f_1, f_2, f_3 and $\sigma_1, \sigma_2, \sigma_3$ are respectively the fractions and the widths of the three gaussians ($f_1 + f_2 + f_3 = 1$). Δ is a mass scale parameter that is left free to be determined by the fit. We also introduced a free

scale parameter (s) in the likelihood fit, multiplying the width of the three gaussians, to account for differences between data and MC. Fig. 15 show the invariant mass distribution of the simulated $B^- \to D^0\pi^-$ events, while Fig. 16 show the invariant mass distribution of the simulated $B^- \to D^0K^-$ events, both with the superimposition of the fit function 5.

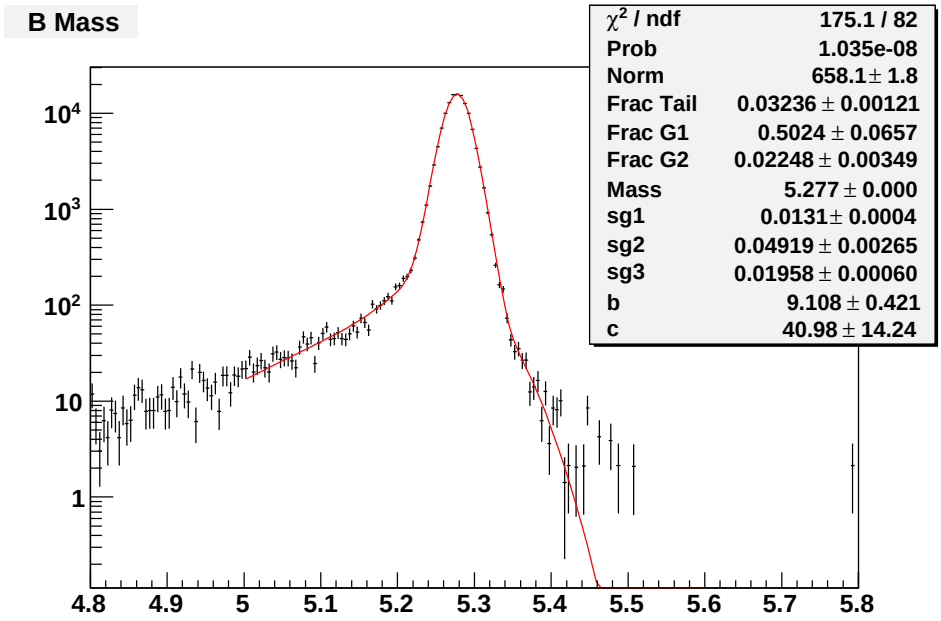

Figure 15: MC simulation, PHOTOS turned on: invariant mass distribution of the simulated $B^+ \to \overline{D}^0\pi^+$ events on logarithmic scale. We overlaided the fit function 5.

8.2 Physics background

8.2.1 $B^+ \to \overline{D}^{*0}\pi^+$

As defined in section 5, the fit window is [5.17, 6.5] GeV/c^2 to have as physics background only the $B^+ \to \overline{D}^{*0}\pi^+$ contribution in CF sample. In Fig. 17 the invariant mass distribution of $D^{0*}\pi$ (log-scale), of MC events, is shown. The distribution has been fitted in the window [5.14,5.6] GeV/c^2 with three gaussians plus an exponential.

8.2.2 Three-body decay

Fig. 18 show the invariant mass distribution of $B^- \to K^-\pi^+\pi^-$ from MC simulation. The decay is reconstructed as $B^- \to D_{DCS}\pi^-$. The distribution has been fitted with two gaussians.

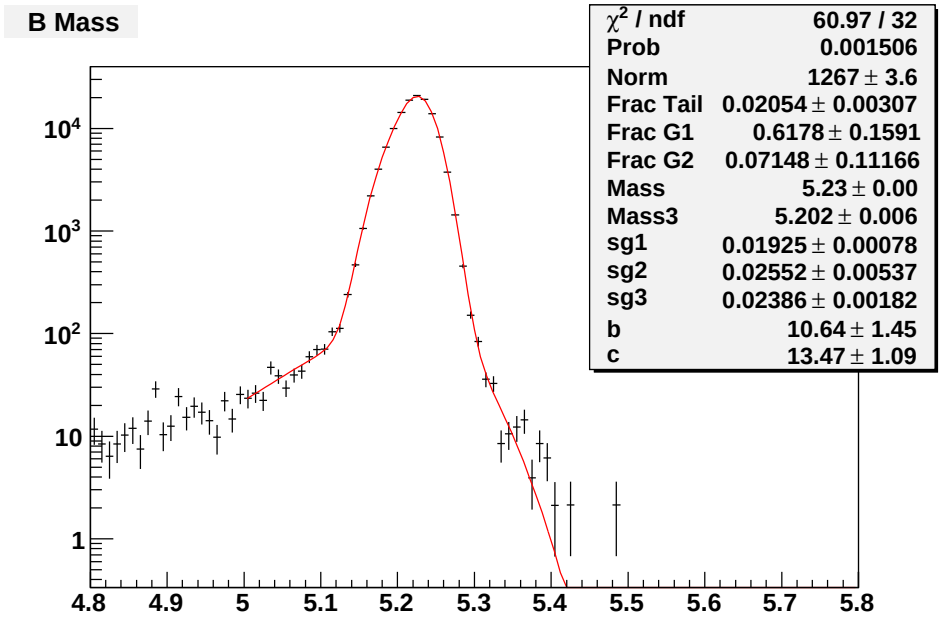

Figure 16: MC simulation, PHOTOS turned on: invariant mass distribution of the simulated $B^+ \to \overline{D}^0 K^+$ events on logarithmic scale. We overlaided the fit function (5).

8.2.3 $B \to D\pi$ with $D \to X$

The $B^- \to D^0\pi^-$ decay with $D^0 \to X$ is reconstructed as $B^- \to D_{DCS}\pi^-$. Fig. 19 shows the invariant mass distribution of this background with superimposed the fit function (a Pearson function of IV type).

8.2.4 $B \to DK$ with $D \to X$

The $B^- \to D^0K^-$ decay with $D^0 \to X$ is reconstructed as $B^- \to D_{DCS}\pi^-$. Fig. 20 shows the invariant mass distribution of this background with superimposed the fit function (one gaussian).

8.2.5 $B^0 \to D_0^{*-}e^+\nu_e$

The $B^0 \to D_0^{*-}e^+\nu_e$, with $D_0^{*-} \to \bar{D^0}\pi^-$, with $\bar{D^0} \to K^+\pi^-$ is reconstructed as $B^- \to D_{DCS}\pi^-$. Fig. 21 shows the invariant mass distribution of this background with superimposed the fit function (one gaussian).

8.3 Combinatorial background

We described the combinatorial background mass shape with an exponential. The slope and the normalization of the exponential are left free in the main fit. We considered

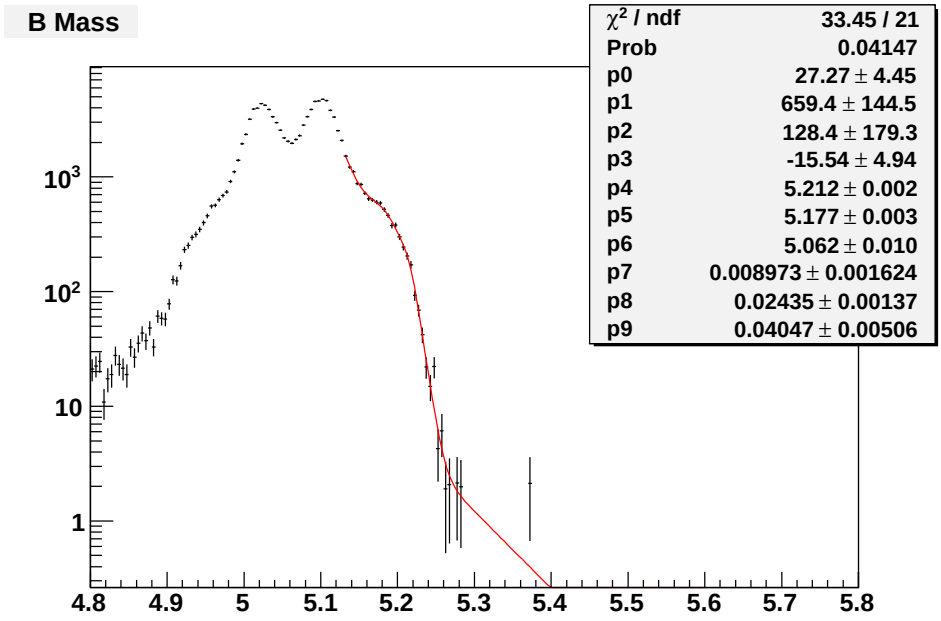

Figure 17: MC simulation, PHOTOS turned on: invariant mass distribution of the simulated $B^+ \to \overline{D}^{0*}\pi^+$ events on logarithmic scale. We overlaided the fit function (three gaussians plus an exponential).

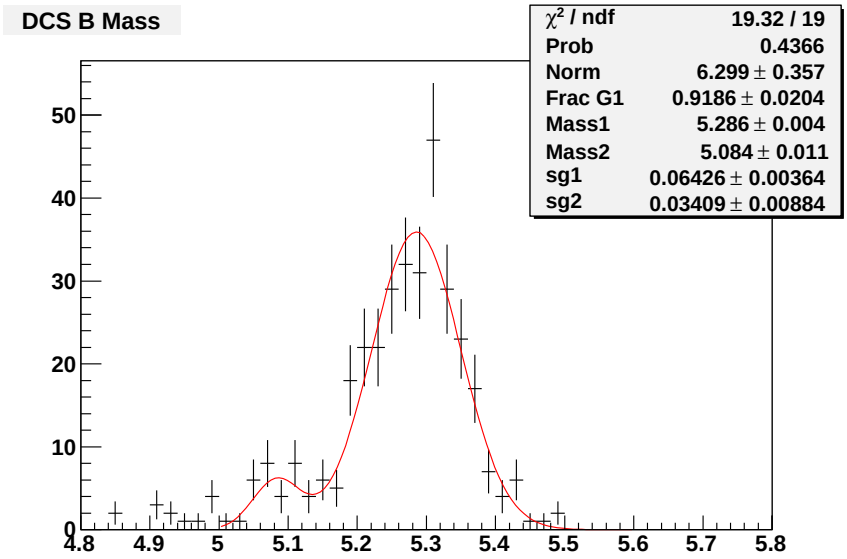

Figure 18: MC simulation, PHOTOS turned on: invariant mass distribution of the simulated $B^- \to K^-\pi^+\pi^-$ events. We overlaided the fit function (two gaussians).

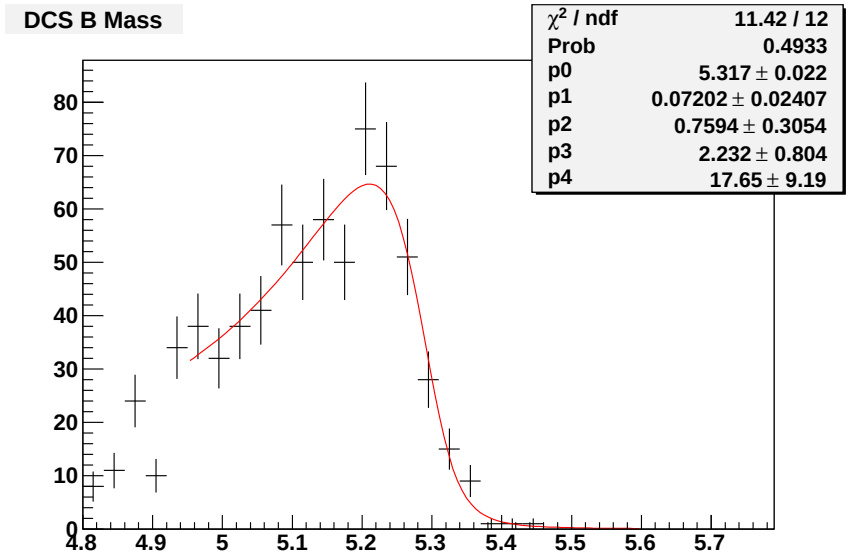

Figure 19: MC simulation, PHOTOS turned on: invariant mass distribution of the simulated $B^- \to D^0\pi^-$ with $D^0 \to X$ events. We overlaided the fit function (a Pearson function of IV type).

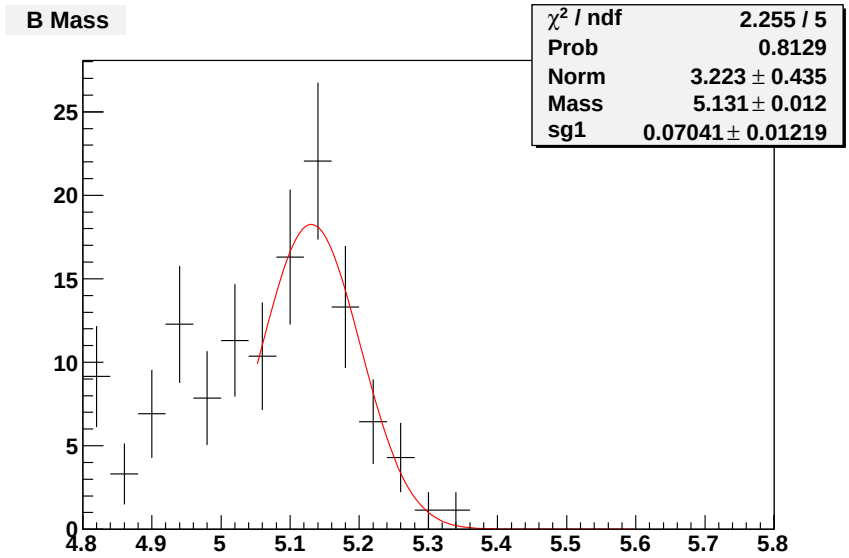

Figure 20: MC simulation, PHOTOS turned on: invariant mass distribution of the simulated $B^- \to D^0K^-$ with $D^0 \to X$ events. We overlaided the fit function (one gaussian).

different shapes for each decay mode, but same slope for positive and negative of the same mode.

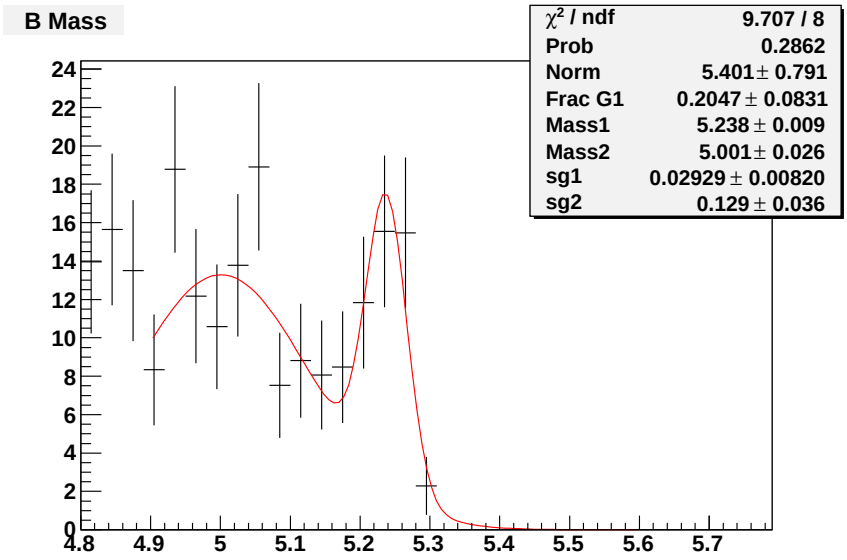

Figure 21: MC simulation, PHOTOS turned on: invariant mass distribution of the simulated $B^0 \to D_0^{*-} e^+ \nu_e$, with $D_0^{*-} \to \bar{D^0}\pi^-$, with $\bar{D^0} \to K^+\pi^-$ events. We overlaided the fit function (one gaussian).

9 PID parameterization (signal and background)

To distinguish between $B \to DK$ and $B \to D\pi$ modes, particle identification is applied to the track from the B. Since that track has $p_T > 2$ GeV/c^2, we can use dE/dx information, obtained from dE/dx calibrations and Universal Curve (UC).
We use official calibrations, blessed by the B-Group [15], while the UC are extrapolated in a pure sample of $D^* \to D^0\pi$, with $D^0 \to K\pi$, using data collected up to p28 (about 6 fb^{-1} of integrated luminosity). Those UC are not yet blessed, but there are plans to be blessed soon.

The motivation to have new UC is that we need to have consistent UC for each sample of data, since we know that dE/dx performances degraded over time. For this reason, blessed UC are not valid up to p31, since they have been performed up to p17 and extended up to p25.
Superimposing new and old UC we can see a shift one respect to the other, which disappears when the two UC are compared in the sub-sample up to p17. Because of this, we think the new UC are correct to be used. Also we verified that these distributions remain unchanged and valid also up to p31.

The PID information can be represented by the single observable κ, defined in section 3.2:

$$\kappa = \frac{\frac{dE}{dx}_{meas} - \frac{dE}{dx}_{exp}(\pi)}{\frac{dE}{dx}_{exp}(K) - \frac{dE}{dx}_{exp}(\pi)}. \tag{6}$$

where $\frac{dE}{dx}_{meas}$ is the measured energy lost by the charged particle in the drift chamber volume and $\frac{dE}{dx}_{exp}(\pi, K)$ is the corresponding expected value in a given particle hypothesis. The average κ, respectively in pion and kaon hypothesis is $< \kappa >_\pi = 0$ and $< \kappa >_K = 1$. This variable take advantage of the fact that is, at the first order, momentum independent.

We determined the pdfs of the κ variable directly from our data-sample. We selected kaons and pions from the D^0 of the B^+ decay, requiring both the pion and the kaon from D^0 to be trigger tracks. We didn't use the residual parameterization blessed by the B-Group because, again, that parameterization was done up to period 17 and we are using data up to period 31.
Parameterizing this variable in our sample it allows us to take into account any systematic effect due to the fact that the UC are not extracted in our sample and to avoid sample dependence effects. This is because the PID templates are constructed in the same data that we fit.

Then we reweighted the transverse momentum distribution (p_t) of kaons and pions from D^0 with the p_t of kaons and pions from B^+. The p_t distributions of kaons and pions from D^0 are taken from data, while the p_t distributions of kaons and pions from B^+ are taken from MC (in the section 4 Fig. 12 show the good agreement between data and MC for the p_t distribution of the track from B). This reweighting is necessary due to the fact that the kaon-pion separation is momentum dependent so we can parameterize the κ distribution using kaons and pions from D^0 but only after the p_t reweighting.

Fig. 22 shows the κ distribution, for pions on the left and for kaons on the right after the reweighting. The two distribution have been fitted using three gaussians. We are

going to use this parameterization in the maximum likelihood fit.

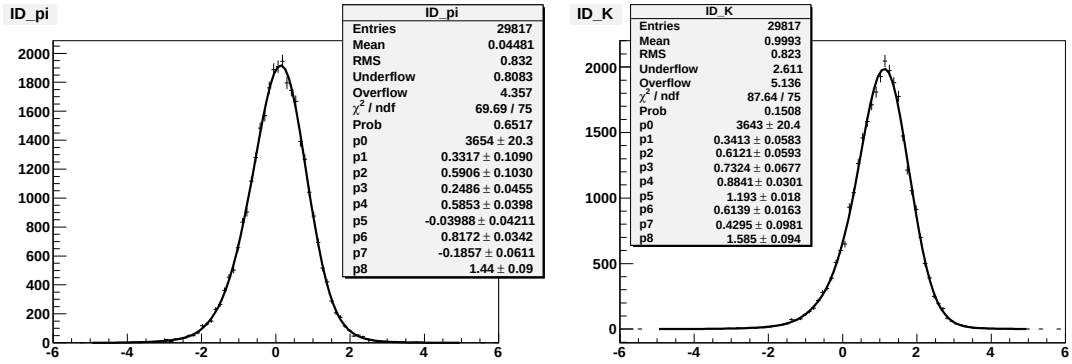

Figure 22: Left: ID distribution for the pion from D^0 from B^+. Right: ID distribution for the kaon from D^0 from B^+. The fit functions are superimposed.

Assuming that the combinatorial background is composed only of pions and kaons, the corresponding PID pdf has the form:

$$a \cdot pdf_\pi(\kappa) + (1-a) \cdot pdf_K(\kappa) \tag{7}$$

where a is the fraction of pions in the combinatorial background. This fraction is left free to float in the maximum likelihood fit.

10 Uncorrected fit results

The fit is performed on the sample selected with the optimized cuts (Fig. 6), with the invariant mass distribution of the B-candidate in the range $5.17 \leq m_{D^0\pi} \leq 6.5$ GeV/c^2. The results of the fit are:

$$\begin{aligned}
R_{ADS}(\pi)_{raw} &= (2.8 \pm 0.7\ (stat.)) \cdot 10^{-3} \\
R_{ADS}(K)_{raw} &= (22.2 \pm 8.6\ (stat.)) \cdot 10^{-3} \\
A_{ADS}(\pi)_{raw} &= 0.13 \pm 0.25\ (stat.) \\
A_{ADS}(K)_{raw} &= -0.82 \pm 0.44\ (stat.) \\
R^+(\pi)_{raw} &= (2.4 \pm 1.0\ (stat.)) \cdot 10^{-3} \\
R^-(\pi)_{raw} &= (3.1 \pm 1.1\ (stat.)) \cdot 10^{-3} \\
R^+(K)_{raw} &= (42.6 \pm 13.7\ (stat.)) \cdot 10^{-3} \\
R^-(K)_{raw} &= (3.8 \pm 10.3\ (stat.)) \cdot 10^{-3}
\end{aligned} \tag{8}$$

We label with the subscript "raw" the fit output which has not yet been corrected for the relative efficiencies.

In table 1 we quote the yields for each decay. The error on the yield is obtained propagating the errors on the fractions and on the numbers of fitted events, according to the formula:

$$Var(y) = \sum_{i=1}^{n}\sum_{j=1}^{n} \frac{\partial y}{\partial x_i}\frac{\partial y}{\partial x_j} \mid_{\vec{c}=\vec{\mu}} (Var(\vec{x}))_{i,j} \tag{9}$$

The same formula is applied also to calculate the errors on the observables ($R_{ADS}(\pi, K)$ and $A_{ADS}(\pi, K)$), that are expressed as functions of the fractions and total numbers of events in each subsample.

Parameter	fraction	yield
$B^+ \to \overline{D}^0\pi^+$ (f_π^{CF+})	0.904 ± 0.004	9882 ± 103
$B^- \to D^0\pi^-$ (f_π^{CF-})	0.893 ± 0.004	9892 ± 103
$B^+ \to \overline{D}^0 K^+$ (f_K^{CF+})	0.063 ± 0.004	694 ± 39
$B^- \to D^0 K^-$ (f_K^{CF-})	0.069 ± 0.004	767 ± 41
$B^+ \to \overline{D}^0\pi^+$ (f_π^{DCS+})	0.44 ± 0.12	24 ± 9
$B^- \to D^0\pi^-$ (f_π^{DCS-})	0.88 ± 0.20	31 ± 10
$B^+ \to \overline{D}^0 K^+$ (f_K^{DCS+})	0.55 ± 0.13	29 ± 9
$B^- \to D^0 K^-$ (f_K^{DCS-})	0.08 ± 0.20	3 ± 8

Table 1: Raw results from the maximum likelihood fit.

Decay	Yield
$B^+ \to D^{0*}\pi^+$ CF	355 ± 27
$B^- \to \overline{D}^{0*}\pi^-$ CF	415 ± 29
$B^+ \to D^{0*}\pi^+$ DCS	1 ± 1
$B^- \to \overline{D}^{0*}\pi^-$ DCS	1 ± 1
$B^+ \to D^0\pi^+$ with $D^0 \to X$	50 ± 7
$B^- \to D^0\pi^-$ with $D^0 \to X$	50 ± 7
$B^+ \to D^0 K^+$ with $D^0 \to X$	1 ± 1
$B^- \to D^0 K^-$ with $D^0 \to X$	2 ± 2
$B^+ \to K^+\pi^-\pi^+$	5 ± 2
$B^- \to K^-\pi^-\pi^+$	6 ± 2
$B^0 \to D_0^{*-} e^+ \nu_e$	2 ± 2
$B^0 \to D_0^{*+} e^- \bar{\nu}_e$	3 ± 2

Table 2: Other parameters resulting from the fit.

Parameter	Value
c^+	0.034 ± 0.003
c^-	0.041 ± 0.003
background fraction (CF pos) (b_{CF+})	0.026 ± 0.002
background fraction (CF neg) (b_{CF-})	0.025 ± 0.002
background fraction (DCS pos) (b_{DCS+})	0.86 ± 0.03
background fraction (DCS neg) (b_{DCS-})	0.90 ± 0.03
$B^+ \to D^0\pi^+$ with $D^0 \to X$ ($f^+_{[X]\pi}$)	0.16 ± 0.01
$B^- \to D^0\pi^-$ with $D^0 \to X$ ($f^-_{[X]\pi}$)	0.15 ± 0.01
$B^+ \to D^0K^+$ with $D^0 \to X$ ($f^+_{[X]K}$)	0.005 ± 0.001
$B^- \to D^0K^-$ with $D^0 \to X$ ($f^-_{[X]K}$)	0.005 ± 0.001
$B^+ \to K^+\pi^-\pi^+$ ($f^+_{K\pi\pi}$)	0.017 ± 0.001
$B^- \to K^-\pi^-\pi^+$ ($f^-_{K\pi\pi}$)	0.016 ± 0.001
$B^0 \to D_0^{*-}e^+\nu_e$ ($f^+_{B^0}$)	0.007 ± 0.003
$B^0 \to D_0^{*+}e^-\bar{\nu}_e$ ($f^-_{B^0}$)	0.007 ± 0.003
f_π in the comb. back (CF & DCS)	0.69 ± 0.03
slope (CF & DCS)	-2.6 ± 0.1
Δ	$(3 \pm 1) \cdot 10^{-4}$
Scale (s)	1.107 ± 0.008

Table 3: Other parameters resulting from the fit.

11 Fit checks

11.1 Toys for the fit consistency

In order to test the fit consistency we used Toy MC. We generated 1000 toys with the fractions and number of events obtained from data (see Table 8). We evaluated the residuals (fitted value − input value) for all four observable and we fitted them with a gaussian function.

The results are shown in Figs. 23, 24.

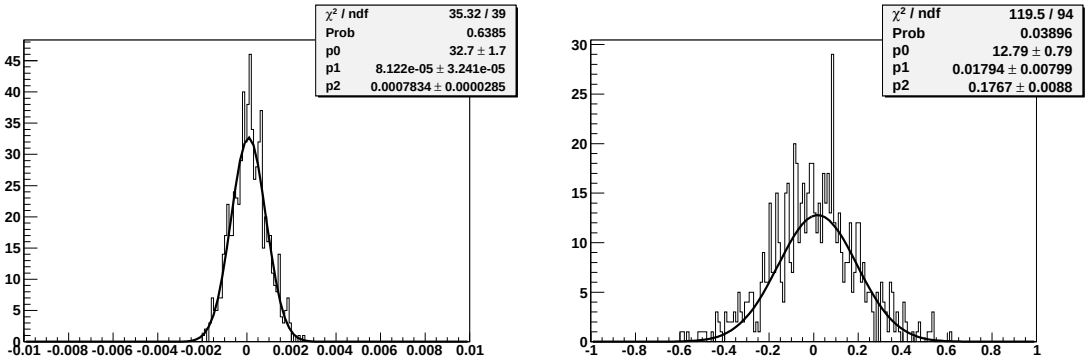

Figure 23: Residuals of $R_{ADS}(\pi)$ (left) and $A_{ADS}(\pi)$ (right) fitted with a gaussian. "p1" is the mean and"p2" is the sigma of the gaussian.

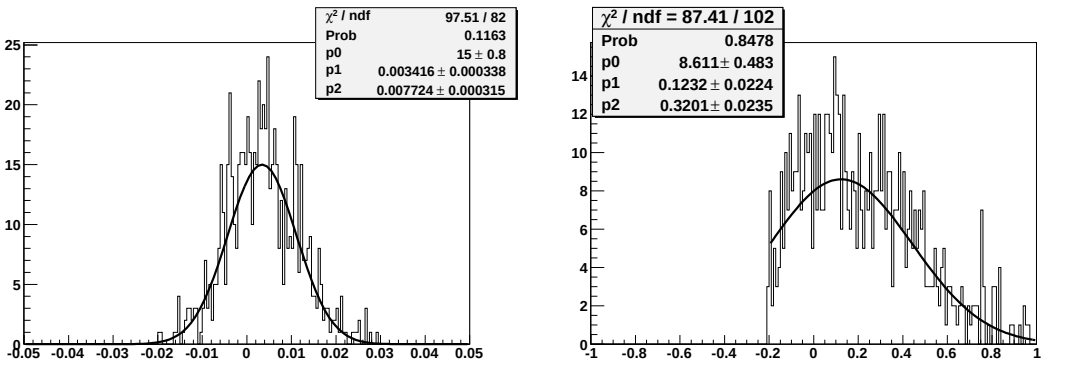

Figure 24: Residuals of $R_{ADS}(K)$ (left) and $A_{ADS}(K)$ (right) fitted with a gaussian."p1" is the mean and"p2" is the sigma of the gaussian.

Looking at the mean and sigma of the residuals, we can evaluate the bias (the "p1" value) and express it as fraction of sigma (the"p2" value). For $R_{ADS}(\pi)$ the bias is $8 \cdot 10^{-5}$, which corresponds to $1/10\sigma$. For $R_{ADS}(K)$ the bias is 0.007, which corresponds to $1/2\sigma$. For $A_{ADS}(\pi)$ the bias is 0.018, which corresponds to $1/10\sigma$. For $A_{ADS}(K)$ the bias is 0.12, which corresponds to $1/3\sigma$.

We can easily see that the residual of the asymmetry of the kaon is cut at the value -0.2. This limit point comes from the boundaries in the asymmetry, that has to lie in the range $[-1, 1]$. Also, the toys are generated with fractions found on data, with the asymmetry very close to -1 and the low statistics spread the distribution making more visible the limit point.
This boundary exist also in the other residual distributions, R for example has to be in the range $[0, 1]$, but it is less visible.

We generated more events in the toys, in particular 10 and 20 times the statistic on data. The residuals for the first case are in Figs. 25 and 26, while for the second are in Figs. 27 and 28. We found a reduction in the width of the residuals and also a reduction in the bias for the kaon observables, while for the pion the bias looks to remain constant. Since the latter is still negligible for our data statistics, we are not going to correct for it.

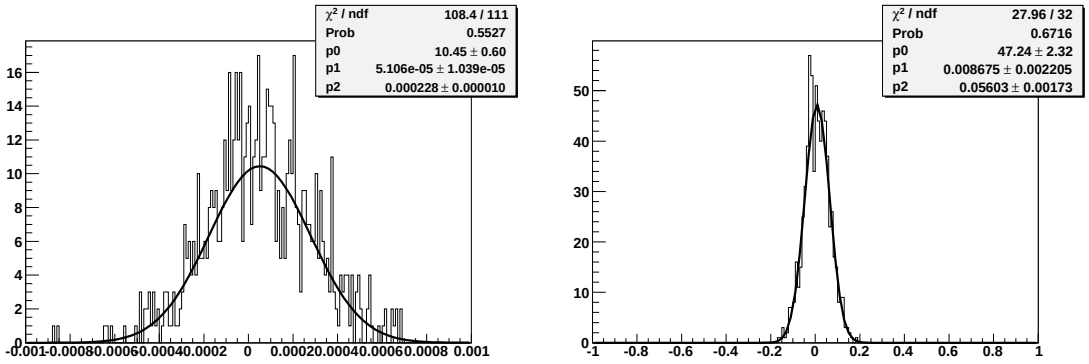

Figure 25: Residuals of $R_{ADS}(\pi)$ (left) and $A_{ADS}(\pi)$ (right), with a statistics 10 times greater than in data, fitted with a gaussian."p1" is the mean and "p2" is the sigma of the gaussian.

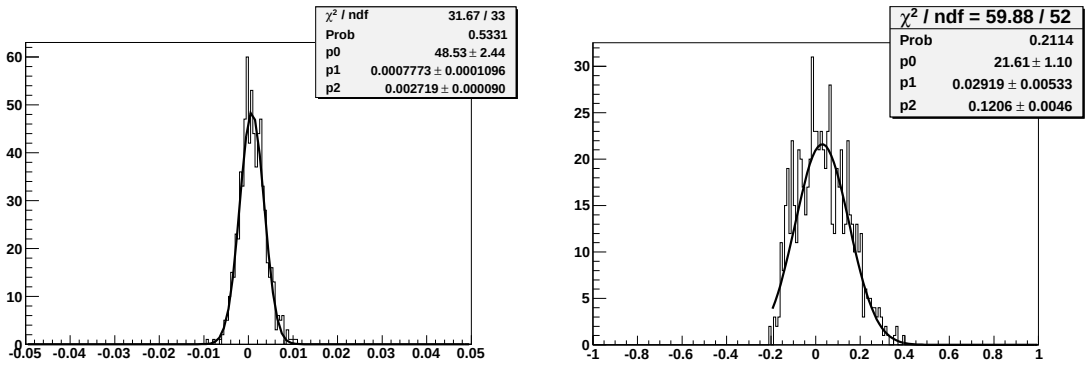

Figure 26: Residuals of $R_{ADS}(K)$ (left) and $A_{ADS}(K)$ (right), with a statistics 10 times greater than in data, fitted with a gaussian. "p1" is the mean and "p2" is the sigma of the gaussian.

We found that the reason of the bias is due to the boundary in the $B \to D^0_{DCS}K$ fraction, which, up to now, has to be in the range $[0, 1]$. This cause the limited residual

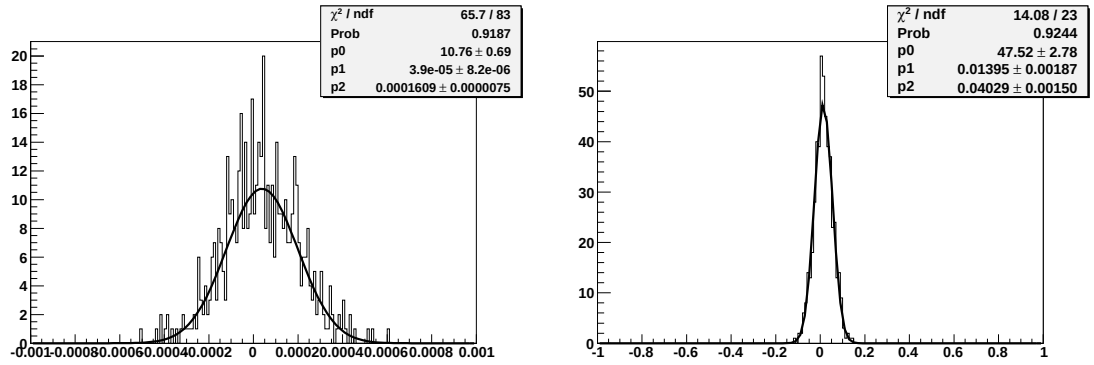

Figure 27: Residuals of $R_{ADS}(\pi)$ (left) and $A_{ADS}(\pi)$ (right), with a statistics 20 times greater than in data, fitted with a gaussian. "p1" is the mean and "p2" is the sigma of the gaussian.

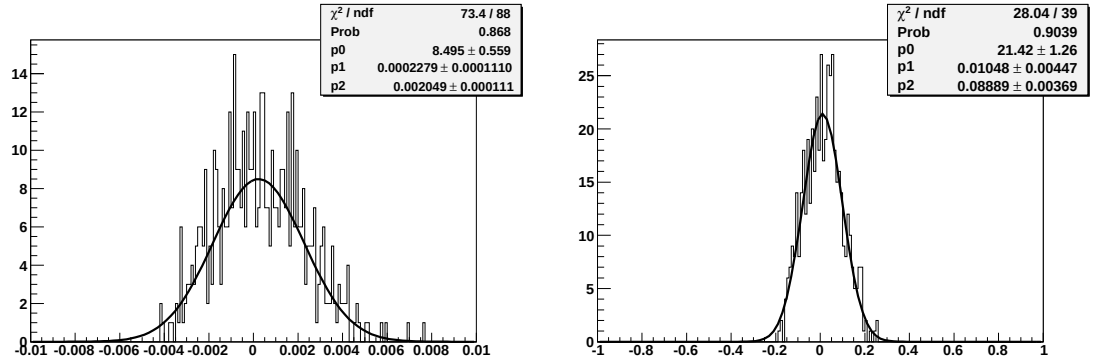

Figure 28: Residuals of $R_{ADS}(K)$ (left) and $A_{ADS}(K)$ (right), with a statistics 20 times greater than in data, fitted with a gaussian. "p1" is the mean and "p2" is the sigma of the gaussian.

distributions and also the bias. We generated toys with the fraction of $B \to D^0_{DCS}K$ floating in the range $[-1, 1]$. The residuals are shown in Figs. 29 and 30 and we can now clearly see that there is no bias nor boundaries in the distributions. We checked that the fit with the fraction of $B \to D^0_{DCS}K$ in $[-1, 1]$ return on data the same results as in the case of $[0, 1]$.

We can conclude that our fit has a bias due to the physical boundary in the fraction of $B \to D^0_{DCS}K$ signal to be greater than 0. But since, after removing this boundary, the fit results remain unchanged and the bias disappear, we do not correct for any bias.

11.2 Likelihood profile

We performed the likelihood profile of the two fractions of $B \to D_{DCS}K$ positive and negative, minimizing the other parameters at each point. In the Fig. 31 we can see the Likelihood profile at one (red), two (green) and three (blue) sigmas. No suspicious behavior appear from the profile.

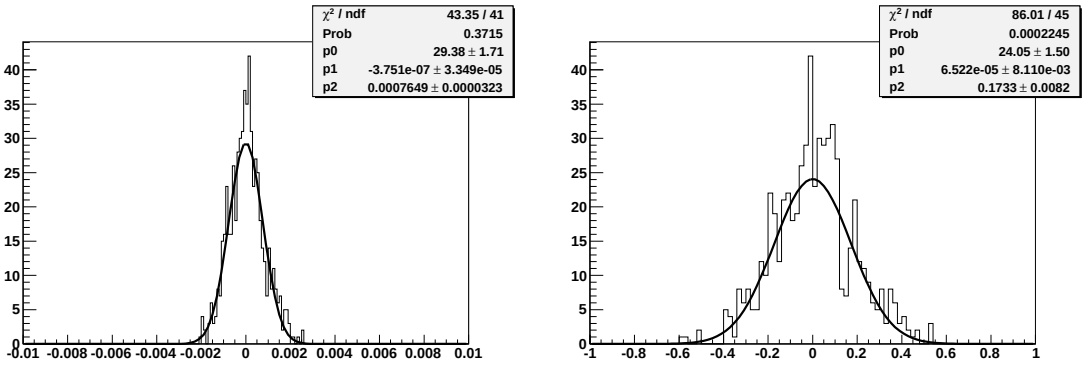

Figure 29: Residuals of $R_{ADS}(\pi)$ (left) and $A_{ADS}(\pi)$ (right), with the same statistics on data and the fraction of $B \to D^0_{DCS}K$ floating in $[-1, 1]$ range in the fit, fitted with a gaussian. "p1" is the mean and "p2" is the sigma of the gaussian.

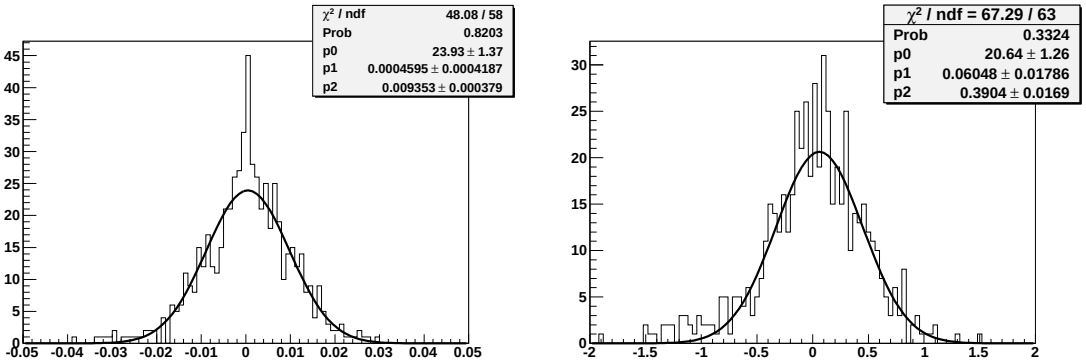

Figure 30: Residuals of $R_{ADS}(K)$ (left) and $A_{ADS}(K)$ (right), with the same statistics on data and the fraction of $B \to D^0_{DCS}K$ floating in $[-1, 1]$ range in the fit, fitted with a gaussian. "p1" is the mean and "p2" is the sigma of the gaussian.

11.3 Correlation matrix

In Fig. 32 we can see the correlation matrix as returned by the fit, where the parameters correspond to:
p1 fraction of CF+ background
p2 fraction of DCS+ background
p3 fraction of CF- background
p4 fraction of DCS- background
p5 fraction of $B \to D\pi$ CF+
p6 fraction of $B \to DK$ DCS+
p7 fraction of $B \to D\pi$ CF-
p8 fraction of $B \to DK$ DCS-
p9 constant $(B \to D^*\pi)/(B \to D\pi)$ pos
p10 constant $(B \to D^*\pi)/(B \to D\pi)$ neg

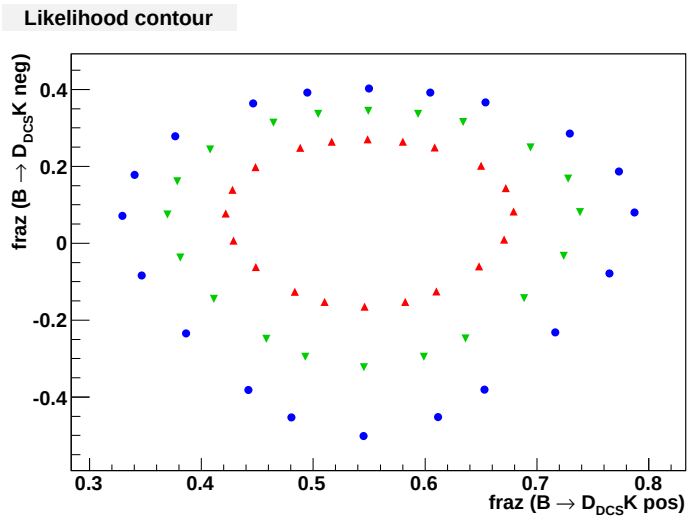

Figure 31: Likelihood profiles for the $B \to DK$ DCS pos vs neg fractions at the level of one (red), two (green) and three (blue) sigmas.

p11 fraction of $B \to [X]_D K$ pos background
p12 fraction of $B \to [X]_D K$ neg background
p13 fraction of $B \to [X]_D \pi$ pos background
p14 fraction of $B \to [X]_D \pi$ neg background
p15 fraction of $B \to K\pi\pi$ pos background
p16 fraction of $B \to K\pi\pi$ neg background
p17 fraction of $B^0 \to D^{*-} e\nu$ pos background
p18 fraction of $B^0 \to D^{*-} e\nu$ neg background
p21 slope of the combinatorial background
p23 fraction of π in the combinatorial background
p27 total number of CF+ events
p28 total number of CF- events
p29 total number of DCS+ events
p30 total number of DCS- events

PARAMETER CORRELATION COEFFICIENTS

NO.	GLOBAL	1	2	3	4	5	6	7	8	9	10	11	12	13	14	15	16
1	0.33343	1.000	0.070	0.090	0.079	0.095	0.009	0.019	-0.051	-0.084	-0.018	-0.036	-0.022	-0.081	-0.062	-0.068	-0.051
2	0.91347	0.070	1.000	0.070	0.064	0.028	0.135	0.009	-0.044	-0.036	0.000	-0.141	-0.019	-0.514	-0.050	-0.439	-0.041
3	0.32417	0.090	0.070	1.000	0.075	0.019	0.008	0.089	-0.045	-0.019	-0.079	-0.019	-0.037	-0.057	-0.083	-0.048	-0.069
4	0.91040	0.079	0.064	0.075	1.000	0.012	0.000	0.033	-0.490	0.001	-0.044	-0.019	-0.146	-0.050	-0.503	-0.042	-0.426
5	0.50132	0.095	0.028	0.019	0.012	1.000	0.014	0.004	-0.015	-0.404	-0.003	-0.201	-0.004	0.039	-0.011	0.033	-0.009
6	0.17462	0.009	0.135	0.008	0.000	0.014	1.000	-0.007	0.012	-0.026	0.012	-0.029	-0.001	-0.058	-0.004	-0.048	-0.003
7	0.51051	0.019	0.009	0.089	0.033	0.004	-0.007	1.000	-0.008	-0.003	-0.418	-0.003	-0.198	-0.009	0.039	-0.008	0.033
8	0.50915	-0.051	-0.044	-0.045	-0.490	-0.015	0.012	-0.008	1.000	0.010	0.003	0.012	0.055	0.031	0.246	0.026	0.211
9	0.43929	-0.084	-0.036	-0.019	0.001	-0.404	-0.026	-0.003	0.010	1.000	0.002	-0.065	0.002	0.001	0.005	0.000	0.004
10	0.45289	-0.018	0.000	-0.079	-0.044	-0.003	0.012	-0.418	0.003	0.002	1.000	0.002	-0.065	0.005	0.002	0.005	0.001
11	0.37500	-0.036	-0.141	-0.019	-0.019	-0.201	-0.029	-0.003	0.012	-0.065	0.002	1.000	0.005	0.248	0.014	0.211	0.012
12	0.38710	-0.022	-0.019	-0.037	-0.146	-0.004	-0.001	-0.198	0.055	0.002	-0.065	0.005	1.000	0.014	0.263	0.012	0.221
13	0.95391	-0.081	-0.514	-0.057	-0.050	0.039	-0.058	-0.009	0.031	0.001	0.005	0.248	0.014	1.000	0.039	0.772	0.033
14	0.95092	-0.062	-0.050	-0.083	-0.503	-0.011	-0.004	0.039	0.246	0.005	0.002	0.014	0.263	0.039	1.000	0.033	0.760
15	0.80898	-0.068	-0.439	-0.048	-0.042	0.033	-0.048	-0.008	0.026	0.000	0.005	0.211	0.012	0.772	0.033	1.000	0.027
16	0.79931	-0.051	-0.041	-0.069	-0.426	-0.009	-0.003	0.033	0.211	0.004	0.001	0.012	0.221	0.033	0.760	0.027	1.000
17	0.13371	-0.016	-0.048	-0.012	-0.010	0.006	-0.009	-0.002	0.005	0.000	0.002	0.033	0.003	0.122	0.008	0.104	0.007
		1.000	0.002	0.040	-0.011	0.021	0.000	-0.114	-0.002								
18	0.12978	-0.013	-0.010	-0.016	-0.045	-0.003	-0.002	0.006	0.015	0.002	0.000	0.003	0.034	0.008	0.118	0.007	0.100
		0.002	1.000	0.042	-0.007	0.000	0.020	-0.002	-0.111								
21	0.51431	-0.303	-0.241	-0.296	-0.267	-0.066	-0.022	-0.063	0.175	0.060	0.059	0.066	0.074	0.191	0.206	0.160	0.171
		0.040	0.042	1.000	-0.020	0.007	0.007	-0.039	-0.041								
23	0.19892	0.021	-0.005	0.032	-0.047	-0.014	0.104	-0.013	0.147	-0.027	-0.026	0.004	0.013	-0.022	0.005	-0.017	0.006
		-0.011	-0.007	-0.020	1.000	-0.005	-0.004	0.025	0.023								
27	0.47222	-0.002	0.022	-0.002	-0.002	0.000	0.005	-0.001	0.001	0.000	0.001	0.039	0.000	0.131	0.001	0.111	0.001
		0.021	0.000	0.007	-0.005	1.000	0.000	0.003	0.000								
28	0.45740	-0.002	-0.002	-0.002	0.021	-0.001	-0.001	0.000	-0.010	0.001	0.000	0.000	0.041	0.001	0.131	0.001	0.109
		0.000	0.020	0.007	-0.004	0.000	1.000	0.000	0.003								
29	0.94517	0.011	-0.118	0.012	0.009	0.002	-0.027	0.003	-0.003	0.000	-0.006	-0.212	-0.002	-0.721	-0.008	-0.609	-0.006
		-0.114	-0.002	-0.039	0.025	0.003	0.000	1.000	0.002								
30	0.94253	0.013	0.010	0.012	-0.114	0.003	0.003	0.002	0.058	-0.006	0.001	-0.002	-0.228	-0.008	-0.728	-0.007	-0.610
		-0.002	-0.111	-0.041	0.023	0.000	0.003	0.002	1.000								

Figure 32: Correlation matrix of the fitted parameters.

12 Fit projections

In order to visualize the agreement between the fit and the data we report the plots of fit projections. A projection of the generic probability density function $pdf(x, \overrightarrow{y}|\overrightarrow{m})$ on the observable x is the plot of the function $\int_{\overrightarrow{y}} pdf(x, \overrightarrow{y}|\overrightarrow{m})d\overrightarrow{y}$, which can be overlaid to the experimental data with the appropriate normalization.

Figs. 33, 34, 35 and 36 show the fit projections on mass and ID variable respectively for CF sample, positive and negative charges, and DCS sample. The points are data and the solid line are the fit projections. For each projection the plot of the difference between projection and data is shown. The agreement between data and fit function appears satisfactory.

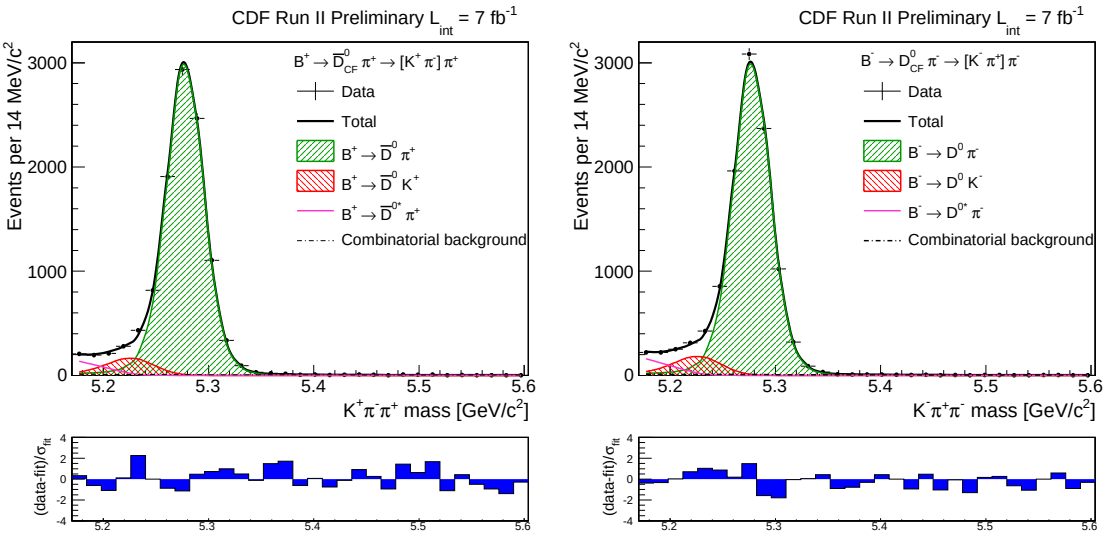

Figure 33: Fit projection in mass range [5.17,5.6] for CF mode positive (left) and negative charges (right).

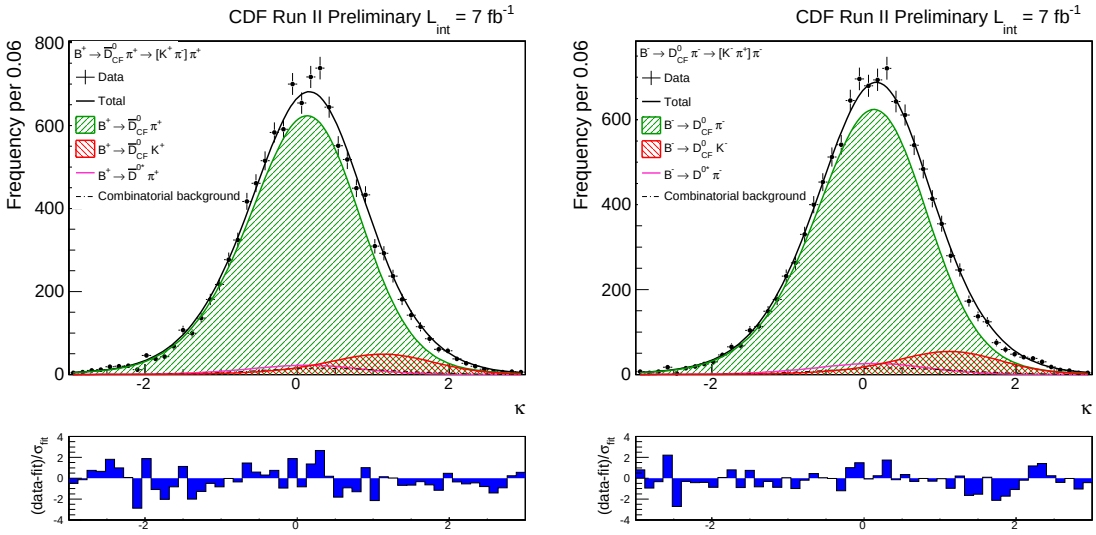

Figure 34: Fit projection in ID range [-3,3] for CF mode positive (left) and negative charges (right).

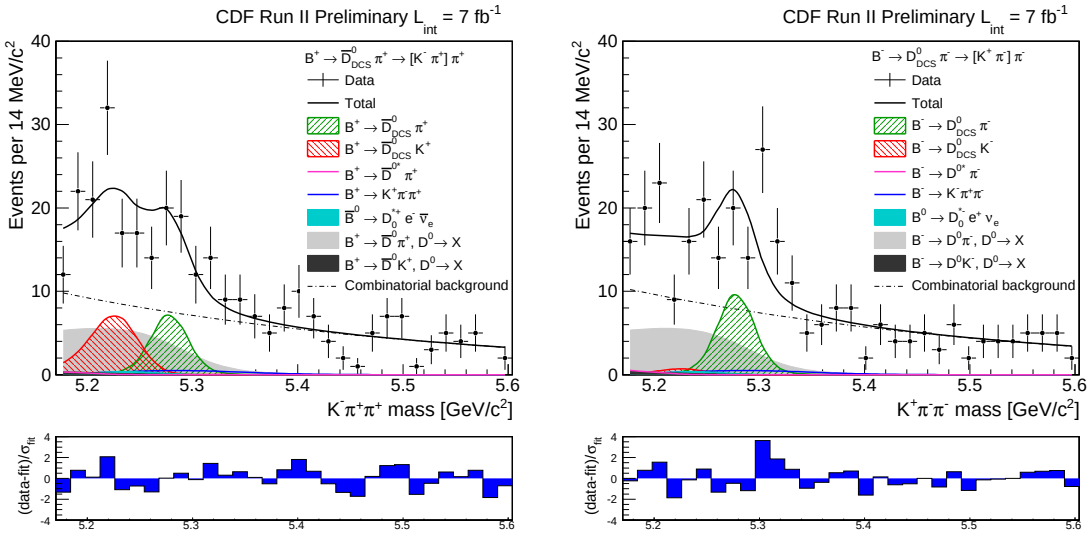

Figure 35: Fit projection in mass range [5.17,5.6] for DCS mode positive (left) and negative charges (right).

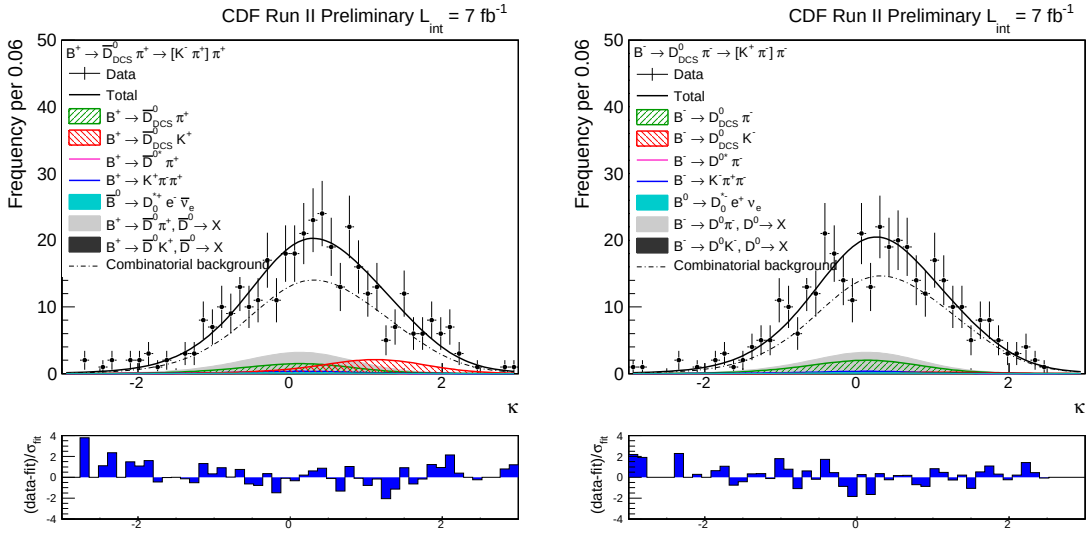

Figure 36: Fit projection in ID range [-3,3] for DCS mode positive (left) and negative charges(right).

13 Efficiency corrections

In order to traslate the raw result of the fit into measurement of relative BRs' and CP asymmetries we need to apply corrections for the different relative efficiencies between the various decay modes.

In the measurement of the direct CP asymmetry the effect of the different hadronic interaction between K^+ and K^- can fake the asymmetry measurement. K^- has a larger hadronic cross section than K^+, and this effect is reproduced rather well by GEANT. We use the results quoted in Tab. 14 of [16] where the following asymmetry is estimated with a careful study on a large Monte Carlo sample. We find:

$$\frac{\epsilon(K^+)}{\epsilon(K^-)} = 1.0178 \pm 0.0023(stat.) \pm 0.0045(syst.). \tag{10}$$

For the pion the efficiency is:

$$\frac{\epsilon(\pi^+)}{\epsilon(\pi^-)} = 0.997 \pm 0.003(stat.), \tag{11}$$

that is fully in agreement with one.

The efficiency of kaon and pion from D^0 is evaluated on our favored $B \to D\pi$ sample and is equal to:

$$\frac{\epsilon(K^-\pi^+)}{\epsilon(K^+\pi^-)} = 0.998 \pm 0.015(stat) \pm 0.016(syst).$$

More details on how we extract this value can be found in the appendix B.

We apply the corrections according to these formulas:

$$\begin{aligned}
\mathcal{R}(h) &= \frac{N_s^- \epsilon(\frac{K^-\pi^+}{K^+\pi^-})\epsilon(\frac{h^+}{h^-}) + N_s^+}{N_f^- \epsilon(\frac{K^+\pi^-}{K^-\pi^+})\epsilon(\frac{h^+}{h^-}) + N_f^+} \\
\mathcal{A}(h) &= \frac{N_s^- \epsilon(\frac{K^-\pi^+}{K^+\pi^-})\epsilon(\frac{h^+}{h^-}) - N_s^+}{N_s^- \epsilon(\frac{K^-\pi^+}{K^+\pi^-})\epsilon(\frac{h^+}{h^-}) + N_s^+} \\
\mathcal{R}^{\pm}(h) &= \frac{N_s^{\pm}}{N_f^{\pm}} \epsilon(\frac{K^{\pm}\pi^{\mp}}{K^{\mp}\pi^{\pm}})
\end{aligned}$$

where $N_s^{\pm}$ are the number of positive and negative suppressed events, $N_f^{\pm}$ are the number of positive and negative favored events and h is pion or kaon.

Corrected results are:

$$\begin{aligned}
R(\pi) &= (2.8 \pm 0.7) \cdot 10^{-3} \\
R(K) &= (22.0 \pm 8.6) \cdot 10^{-3} \\
A(\pi) &= 0.13 \pm 0.25 \\
A(K) &= -0.82 \pm 0.44 \\
R^+(\pi) &= (2.4 \pm 1.0) \cdot 10^{-3}
\end{aligned}$$

$$
\begin{aligned}
R^-(\pi) &= (3.1 \pm 1.1) \cdot 10^{-3} \\
R^+(K) &= (42.6 \pm 13.7) \cdot 10^{-3} \\
R^-(K) &= (3.8 \pm 10.3) \cdot 10^{-3}
\end{aligned}
$$

14 Systematics

In the following sub-sections we will describe the main sources of systematic uncertainties.

14.1 dE/dx

dE/dx information comes in the κ variable, whose distribution is shown in Fig. 22. The distribution is taken from data and fitted with the sum of three gaussian. The nine parameters of the function are correlated according to a certain correlation matrix.

To evaluate the dE/dx systematic we generated several sets of nine random gaussian variables, correlated with the same correlation matrix obtained on data. The numerical algorithm to generate multivariate variables can be found in several books, see for example the Cap. 33 of [17].

For each set of variables we have a different κ curve. In Fig. 37 we superimposed one thousand of these systematic κ curves to data. The curves completely cover the region of data errors.

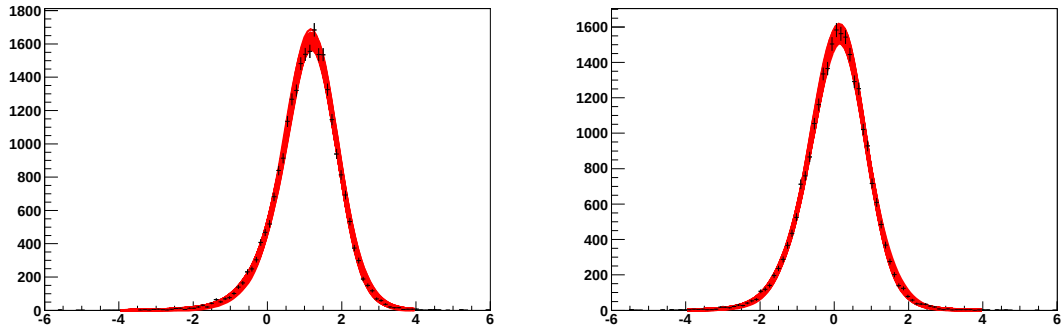

Figure 37: κ variable, on the left for the K, on the right for the π. Points with error bars come from data, while in red are one thousand systematic curves.

In the limit of small errors select a region of one sigma in the parameters of the κ correspond to select a region of one sigma in the observables. For this reason we don't select one sigma in the parameters space, but we will select a one sigma region in the observables space.
To do this we used each systematic curve to fit the data, so that we have a distribution of the observables, as can be seen in Figs. 38 and 39. Fitting them with gaussian functions, we take the sigma of the gaussian as the dE/dx systematic error.

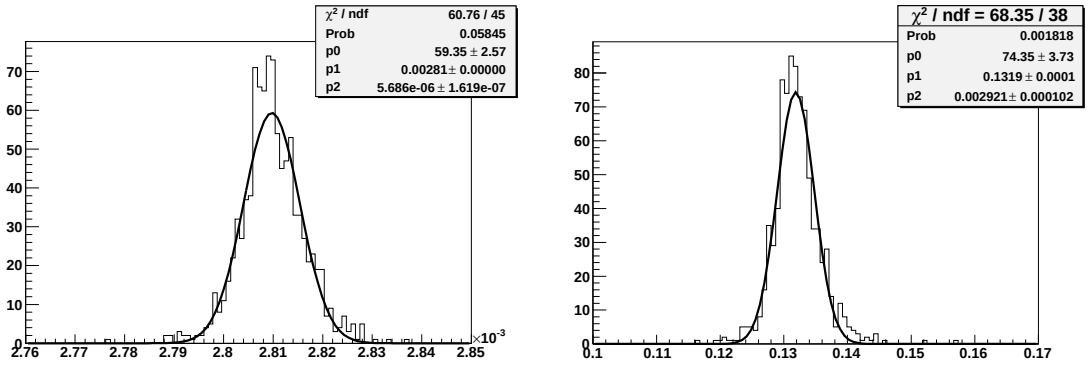

Figure 38: Distributions of $R_{ADS}(\pi)$ (left) and $A_{ADS}(\pi)$ (right) obtained with the systematic curves of dE/dx. They are fitted with a gaussian and the sigma ("p2") is taken as systematic error.

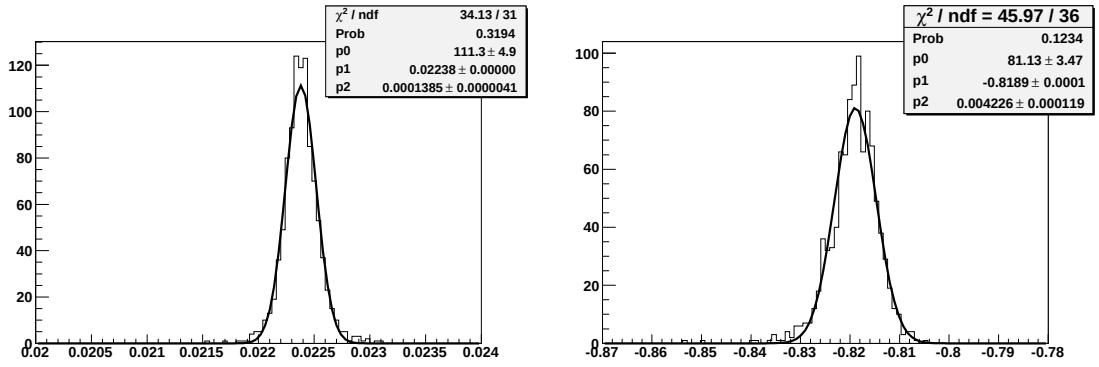

Figure 39: Distributions of $R_{ADS}(K)$ (left) and $A_{ADS}(K)$ (right) obtained with the systematic curves of dE/dx. They are fitted with a gaussian and the sigma ("p2") is taken as systematic error.

14.2 Mass model of the combinatorial background

Our central fit assumes a mass-shape of the combinatorial background events distribuited as an exponential function. We verified that the shape is exponential also under the B peaks, using:

- B events in the D^0 sidebands (3σ) (Fig. 40);
- B events selected with the same cuts of the analysis, but $\chi^2_{3D} \geq 30$.

To evaluate the systematics we redid the fit using different shapes:

- exponential plus constant
- exponential plus first degree polynomial
- exponential plus second degree polynomial

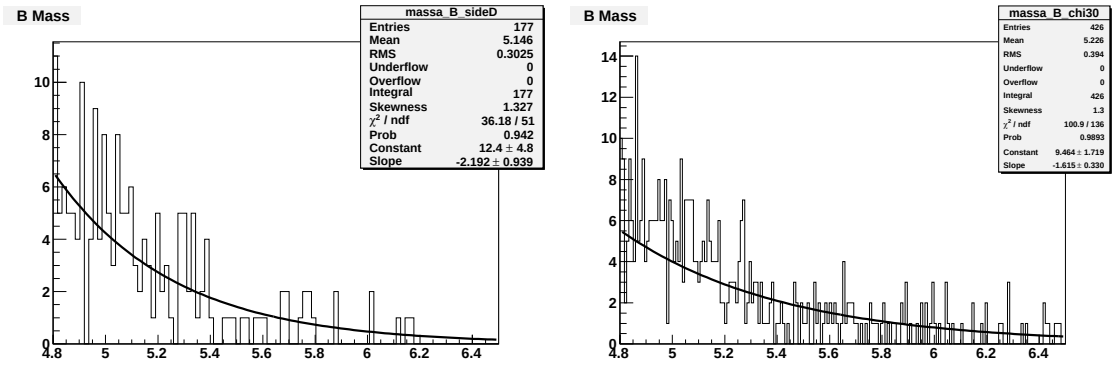

Figure 40: Invariant B mass distribution in the D^0 sidebands (left) and with the $\chi^2_{3D} \geq 30$ (right).

We then take the worse of the three cases, the exponential plus constant. In the other two cases the value of the slope remain constant, while, adding a constant, that value goes from -2.71 ± 0.15 of the central fit to -2.86 ± 0.15.

We used as systematic error the difference between the observables results obtained using the exponential plus constant and the central fit.

14.3 Physics background mass model

To evaluate this systematic, we varied the shape of the physics background.

- $B^- \to D^0\pi$ with $D^0 \to X$
  The mass shape is parametrized with a Pearson function of the IV type, we varied the parameters corresponding to the mean and the width of $\pm 1\sigma$.

- $B^- \to D^0 K$ with $D^0 \to X$
  Since we parametrized the mass shape with a gaussian, we varied the mean and the width of the gaussian of $\pm 1\sigma$.

- $B^- \to K^-\pi^+\pi^-$
  We parametrized the mass shape with two gaussians. To evaluate the systematics we varied the mean and the width of the second gaussian, that is the one goes under the B signal peaks, of $\pm 1\sigma$.

- $B^0 \to D_0^{*-} e^+ \nu_e$
  We parametrized the mass shape with two gaussians. To evaluate the systematics we varied the mean and the width of the second gaussian, that is the one goes under the B signal peaks, of $\pm 1\sigma$.

- $B^- \to D^{*0}\pi^-$
  We parametrized the mass shape with three gaussians plus an exponential. To evaluate the systematics we varied the slope of the exponential of $\pm 1\sigma$.

Source	$R^+_{ADS}(\pi)$	$R^-_{ADS}(\pi)$	$R^+_{ADS}(K)$	$R^-_{ADS}(K)$	$R_{ADS}(\pi)$	$R_{ADS}(K)$	$A_{ADS}(\pi)$	$A_{ADS}(K)$
dE/dx	0.00001	0.00001	0.0003	0.0001	0.00001	0.0001	0.003	0.004
combinatorial background	0.00001	0.00001	0.0001	0.0002	0.00001	0.0001	0.001	0.010
$B^- \to [X]_D\pi^-$ shape	0.00040	0.00040	0.0026	0.0026	0.00038	0.0025	0.013	0.089
$B^- \to [X]_D K^-$ shape	0.00001	0.00001	0.0001	0.0001	0.00001	0.0001	0.000	0.003
$B^- \to K^-\pi^+\pi^-$ shape	0.00002	0.00002	0.0001	0.0001	0.00002	0.0001	0.001	0.003
$B^0 \to D_0^{*-}e^+\nu_e$ shape	0.00004	0.00004	0.0003	0.0002	0.00004	0.0002	0.003	0.007
$B^- \to D^{*0}\pi^-$ shape	0.00004	0.00005	0.0005	0.0004	0.00005	0.0005	0.001	0.014
efficiency of K_B	-	-	-	-	-	0.0001	-	0.002
efficiency of π_B	-	-	-	-	-	-	0.003	-
efficiency of $K_D\pi_D$	0.00005	0.00007	0.0009	0.0001	0.00006	0.0003	0.011	0.004
Total	**0.00041**	**0.00041**	**0.0028**	**0.0027**	**0.00039**	**0.0026**	**0.018**	**0.091**

Table 4: Systematic uncertainties for all observables.

14.4 Total systematic uncertainties

A summary of all systematics is reported in Table 4.

The total systematic uncertainty on each measurement is determined as the sum in quadrature of all systematic uncertainties.

15 Significance evaluation

To evaluate the significance of the $B \to D^0_{DCS}K$ signal we need first of all to repeat the fit fixing to zero the fractions of $B^+ \to \overline{D}^0_{DCS}K^+$ and $B^- \to D^0_{DCS}K^-$ and to calculate the difference of $-2\log\mathcal{L}$ between the central fit and the latter fit. We obtain a $-2\Delta\log\mathcal{L}$, which we will call DLL, of 14.1.

Now we want to include also the systematic variations. To do this we need to find the worse systematic configuration, the one in which the DLL value is closest to zero. The procedure we use is to repeat the fit on data, using each time a different systematic shape and see which of them lowers the DLL. We found that the only three which have an effect are: the dE/dx, the $B \to [X]_D\pi$ and the $B^0 \to D_0^{*-}e^+\nu_e$ shape.
We combined the three, obtaining the distribution in Fig. 41 and we select the configuration giving the lower DLL.

We generated 48000 toys with zero $B \to D^0_{DCS}K$ events as input value and we use for dE/dx and physics background the configuration previously chosen.

We then fit these toys with the central fit, obtaining the distribution of $-2\Delta\log\mathcal{L}$ shown in Fig. 42.

The number of cases with DLL greater than 14.1 is 69, which divided by the total, 46664, corresponds to a p-value of about $1.48 \cdot 10^{-3}$. The resulting significance (including systematics) is 3.2 σ, so we find evidence of $B \to D^0_{DCS}K$ signal.

For the $B \to D^0_{DCS}\pi$ we only evaluate the statistical significance, repeating the fit on data fixing the fraction of $B \to D^0_{DCS}\pi$ equal to zero. The DLL is 16.3, corresponding to a statistical significance of 3.6 σ [4].

[4]To convert a p-value (α) in number of sigma (n), we applied the formula: $n = \sqrt{2} \cdot Erf^{-1}(1-\alpha)$.

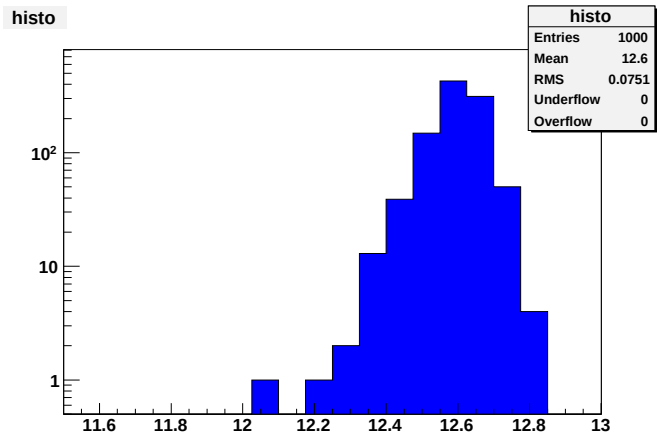

Figure 41: $-2\Delta \log \mathcal{L}$ distribution on data, obtained with various systematic configurations on dE/dx and physics background pdfs.

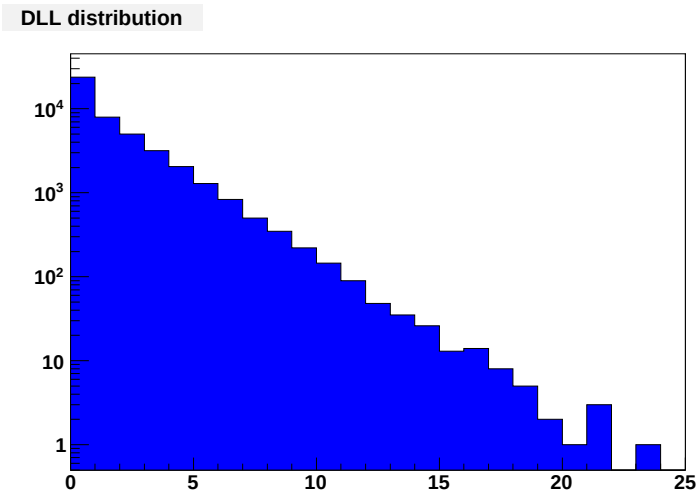

Figure 42: $-2\Delta \log \mathcal{L}$ distribution on toys with zero signal input.

16 Asymmetry of K

Since our value of the kaon asymmetry is close to -1 and about 2σ far from zero, we want to evaluate exactly how much is far from zero and see if it can be significantly different from zero.
For this reason we generate 2000 toys with zero input value of the asymmetry and the other values as found on data. Fitting these toys with our central fit, we obtain the distribution of the asymmetry as in Fig. 43.

The sigma of this distribution is 0.37 and our central value of the asymmetry is 2.2σ far from zero.

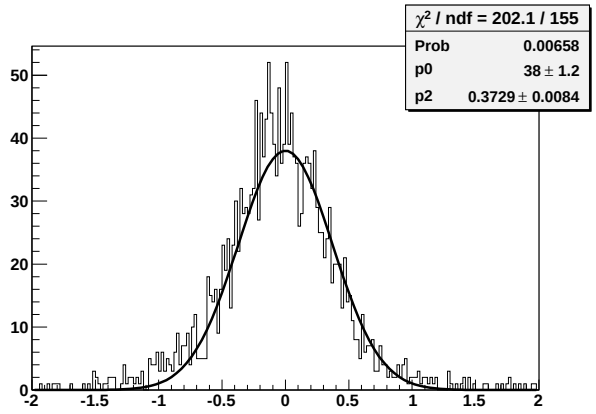

Figure 43: Distribution of the kaon asymmetry, fitted from a toy with zero input value of the asymmetry.

17 Final results

We measure on 7 fb^{-1} of data:

$$\begin{aligned} R_{ADS}(\pi) &= \frac{BR(B^- \to D^0_{DCS}\pi^-) + BR(B^+ \to D^0_{DCS}\pi^+)}{BR(B^- \to D^0_{CF}\pi^-) + BR(B^+ \to D^0_{CF}\pi^+)} = \\ &= (2.8 \pm 0.7\ (stat.) \pm 0.4\ (syst.)) \cdot 10^{-3} \end{aligned}$$

$$\begin{aligned} R_{ADS}(K) &= \frac{BR(B^- \to D^0_{DCS}K^-) + BR(B^+ \to D^0_{DCS}K^+)}{BR(B^- \to D^0_{CF}K^-) + BR(B^+ \to D^0_{CF}K^+)} = \\ &= (22.0 \pm 8.6\ (stat.) \pm 2.6\ (syst.)) \cdot 10^{-3} \end{aligned}$$

$$\begin{aligned} A_{ADS}(\pi) &= \frac{BR(B^- \to D^0_{DCS}\pi^-) - BR(B^+ \to D^0_{DCS}\pi^+)}{BR(B^- \to D^0_{DCS}\pi^-) + BR(B^+ \to D^0_{DCS}\pi^+)} = \\ &= 0.13 \pm 0.25\ (stat.) \pm 0.02\ (syst.) \end{aligned}$$

$$\begin{aligned} A_{ADS}(K) &= \frac{BR(B^- \to D^0_{DCS}K^-) - BR(B^+ \to D^0_{DCS}K^+)}{BR(B^- \to D^0_{DCS}K^-) + BR(B^+ \to D^0_{DCS}K^+)} = \\ &= -0.82 \pm 0.44\ (stat.) \pm 0.09\ (syst.) \end{aligned}$$

$$\begin{aligned} R^+(\pi) &= \frac{BR(B^+ \to D^0_{DCS}\pi^+)}{BR(B^+ \to D^0_{CF}\pi^+)} = \\ &= (2.4 \pm 1.0\ (stat.) \pm 0.4\ (syst.)) \cdot 10^{-3} \end{aligned}$$

$$\begin{aligned} R^-(\pi) &= \frac{BR(B^- \to D^0_{DCS}\pi^-)}{BR(B^- \to D^0_{CF}\pi^-)} = \\ &= (3.1 \pm 1.1\ (stat.) \pm 0.4\ (syst.)) \cdot 10^{-3} \end{aligned}$$

$$\begin{aligned} R^+(K) &= \frac{BR(B^+ \to D^0_{DCS}K^+)}{BR(B^+ \to D^0_{CF}K^+)} = \\ &= (42.6 \pm 13.7\ (stat.) \pm 2.8\ (syst.)) \cdot 10^{-3} \end{aligned}$$

$$R^-(K) = \frac{BR(B^- \to D^0_{DCS} K^-)}{BR(B^- \to D^0_{CF} K^-)} =$$

$$= (3.8 \pm 10.3\ (stat.) \pm 2.7\ (syst.)) \cdot 10^{-3}$$

We find evidence of the signals $B \to D^0 K$ and $B \to D^0 \pi$ DCS, respectively with a significance of 3.2σ (including systematics) and 3.6σ (only statistical).

A Observables for the ADS method

A.1 Definitions

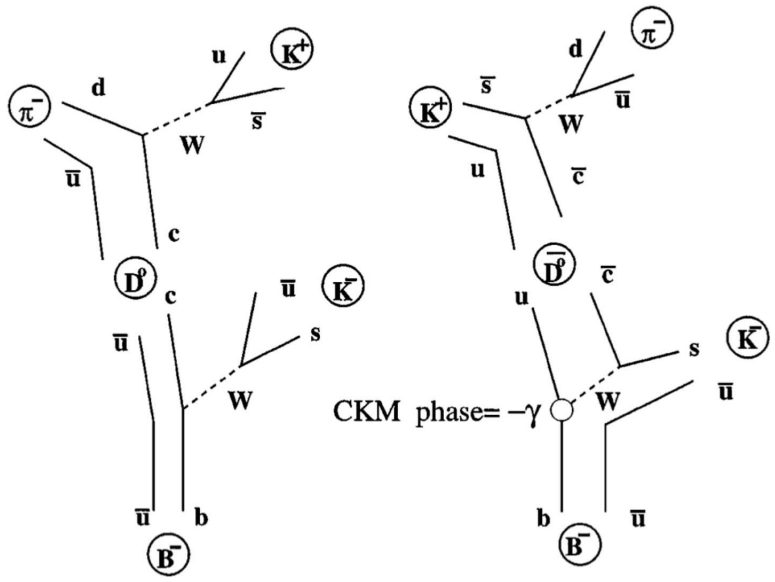

Figure 44: Diagram of the two interfering processes: $B^- \to D^0 K^-$ (color allowed) followed by $D^0 \to K^+\pi^-$ (doubly Cabibbo suppressed) and $B^- \to \overline{D}^0 K^-$ (color suppressed) followed by $\overline{D}^0 \to K^+\pi^-$ (Cabibbo allowed).

Using the notation introduced in [1, 2], we can define the following branching ratios:

$$\begin{array}{ll} a = \mathcal{B}(B^- \to D^0 K^-) & \overline{a} = \mathcal{B}(B^+ \to \overline{D}^0 K^+) \\ b = \mathcal{B}(B^- \to \overline{D}^0 K^-) & \overline{b} = \mathcal{B}(B^+ \to D^0 K^+) \\ c(f) = \mathcal{B}(D^0 \to f) & \overline{c}(\overline{f}) = \mathcal{B}(\overline{D}^0 \to \overline{f}) \\ c(\overline{f}) = \mathcal{B}(D^0 \to \overline{f}) & \overline{c}(f) = \mathcal{B}(\overline{D}^0 \to f) \\ d(f) = \mathcal{B}(B^- \to [f]K^-) & \overline{d}(\overline{f}) = \mathcal{B}(B^+ \to [\overline{f}]K^+) \end{array}$$

where $f = K^+\pi^-$. In the SM we assume that: $a = \overline{a}$, $b = \overline{b}$, $c(\overline{f}) = \overline{c}(f)$ and $\overline{c}(\overline{f}) = \overline{c}(\overline{f})$.

Since the two decay channels of Fig. 44 are indistinguishable, we measure the interference (which is sensible to γ):

$$\begin{aligned} d(f) = \mathcal{B}(B^- \to [f]K^-) &= \mathcal{B}(B^- \to D^0 K^-)\mathcal{B}(D^0 \to f) + \mathcal{B}(B^- \to \overline{D}^0 K^-)\mathcal{B}(\overline{D}^0 \to f) + \\ &\quad 2\sqrt{\mathcal{B}(B^- \to D^0 K^-)\mathcal{B}(D^0 \to f)\mathcal{B}(B^- \to \overline{D}^0 K^-)\mathcal{B}(\overline{D}^0 \to f)} \\ &\quad \cos(\delta + \gamma) \\ &= ac(f) + b\overline{c}(f) + 2\sqrt{ac(f) + b\overline{c}(f)}\cos(\delta + \gamma) \end{aligned} \tag{12}$$

where $\delta = \delta_B + \delta_D$ is the sum of the strong phases.

In the same way we can write:

$$\begin{aligned}\overline{d}(\overline{f}) = \mathcal{B}(B^+ \to [\overline{f}]K^+) &= \mathcal{B}(B^+ \to \overline{D}^0 K^+)\mathcal{B}(\overline{D}^0 \to \overline{f}) + \mathcal{B}(B^+ \to D^0 K^+)\mathcal{B}(D^0 \to \overline{f}) + \\ &\quad 2\sqrt{\mathcal{B}(B^+ \to \overline{D}^0 K^+)\mathcal{B}(\overline{D}^0 \to \overline{f})\mathcal{B}(B^+ \to D^0 K^+)\mathcal{B}(D^0 \to \overline{f})} \\ &\quad \cos(\delta - \gamma) \\ &= ac(f) + b\overline{c}(f) + 2\sqrt{ac(f) + b\overline{c}(f)}\cos(\delta - \gamma) \qquad (13)\end{aligned}$$

which differs from $d(f)$ only for the sign of γ.

In the articles written by Atwood, Dunietz and Soni [1, 2], there is only the definition of *CP violating partial rate asymmetry*:

$$A(f) = \frac{d(f) - \overline{d}(\overline{f})}{d(f) + \overline{d}(\overline{f})} \qquad (14)$$

which exactly corresponds to what we called:

$$\mathcal{A}_{ADS} = \frac{\mathcal{B}(B^- \to [f]K^-) - \mathcal{B}(B^+ \to [\overline{f}]K^+)}{\mathcal{B}(B^- \to [f]K^-) + \mathcal{B}(B^+ \to [\overline{f}]K^+)}$$

There are no definitions of $\mathcal{R}_{ADS}$. How can we get there?. In [1] authors say:

> *... a can be determined via Cabibbo allowed modes of D^0 decay (g), e.g. $D^0 \to K^-\pi^+, K^-\rho^+$. The decay chain $B^- \to D^0[\to g]K^-$ determines $a \approx d(g)/c(g)$ to an accuracy of about 1% since the interfering process $B^- \to \overline{D}^0[\to g]K^-$ is both color and doubly Cabibbo suppressed.*

Using $g = K^-\pi^+ = \overline{f}$, we can write

$$a \approx d(g)/c(g) = d(g)/c(\overline{f})$$

We can easily replace $a = d(g)/c(\overline{f})$ and $c(\overline{f}) = d(g)/a$ in (12) and (13). Calling $r_B^2 = b/a$ and $r_D^2 = c(f)/c(\overline{f})$, we obtain the formulas:

$$\begin{aligned} d(f) &\approx d(g) \cdot [r_B^2 + r_D^2 + 2r_B r_D \cos(\delta + \gamma)] \qquad (15) \\ \overline{d}(\overline{f}) &\approx \overline{d}(\overline{g}) \cdot [r_B^2 + r_D^2 + 2r_B r_D \cos(\delta - \gamma)] \qquad (16)\end{aligned}$$

from which we can define:

$$\begin{aligned} R^- &\equiv \frac{d(f)}{d(g)} = \frac{\mathcal{B}(B^- \to [f]K^-)}{\mathcal{B}(B^- \to [g]K^-)} = \frac{\mathcal{B}(B^- \to [K^+\pi^-]K^-)}{\mathcal{B}(B^- \to [K^-\pi^+]K^-)} \qquad (17) \\ R^+ &\equiv \frac{\overline{d}(\overline{f})}{\overline{d}(\overline{g})} = \frac{\mathcal{B}(B^+ \to [\overline{f}]K^+)}{\mathcal{B}(B^+ \to [\overline{g}]K^+)} = \frac{\mathcal{B}(B^+ \to [K^-\pi^+]K^+)}{\mathcal{B}(B^+ \to [K^+\pi^-]K^+)}. \qquad (18)\end{aligned}$$

They are the ratios between $\mathcal{B}$ of suppressed over favored decay modes for negative and positive charges respectively.
R^+/R^- are not defined in [1, 2], but can easily be extracted using the $\mathcal{B}$.

In the same way we can define also:

$$\mathcal{R}_{ADS} \equiv \frac{d(f)+\overline{d}(\overline{f})}{d(g)+\overline{d}(\overline{g})} = \frac{\mathcal{B}(B^- \to [K^+\pi^-]K^-) + \mathcal{B}(B^+ \to [K^-\pi^+]K^+)}{\mathcal{B}(B^- \to [K^-\pi^+]K^-) + \mathcal{B}(B^+ \to [K^+\pi^-]K^+)} \tag{19}$$

All these definitions with $\mathcal{B}$ look clear and consistent, there is only an approximation coming in the formulas with r_B and r_D.

In [6] or in [18] there are two more definitions, relating R^+, R^-, $\mathcal{R}_{\mathcal{ADS}}$ and $\mathcal{A}_{\mathcal{ADS}}$:

$$\begin{aligned} \mathcal{R}_{ADS} &= \frac{R^+ + R^-}{2} \\ \mathcal{A}_{ADS} &= \frac{R^- - R^+}{R^- + R^+} \end{aligned} \tag{20}$$

Considering the $\mathcal{B}$s they are wrong.

The only way they can be correct is considering the *approximate* relations with r_D and r_B.

$$\begin{aligned} R^- &= r_B^2 + r_D^2 + 2r_B r_D \cos(\delta+\gamma) \\ R^+ &= r_B^2 + r_D^2 + 2r_B r_D \cos(\delta-\gamma) \\ \mathcal{R}_{ADS} &= r_B^2 + r_D^2 + 2r_B r_D \cos(\delta)\cos(\gamma) \\ \mathcal{A}_{ADS} &= 2r_B r_D \sin(\delta)\sin(\gamma)/\mathcal{R}_{ADS} \end{aligned}$$

In this way the equivalences (20) are satisfied.

Also the trivial case, when $R^+ = R^-$ verifies the equations (20).

A.2 Experimental results

Using the same fit technique described in the note, we find these results:

$$\begin{aligned} \mathcal{R}^+_{ADS}(\pi) &= (2.4 \pm 1.0) \cdot 10^{-3} \\ \mathcal{R}^-_{ADS}(\pi) &= (3.1 \pm 1.1) \cdot 10^{-3} \\ \mathcal{R}^+_{ADS}(K) &= (42.6 \pm 13.7) \cdot 10^{-3} \\ \mathcal{R}^-_{ADS}(K) &= (3.8 \pm 10.3) \cdot 10^{-3} \end{aligned}$$

where the statistical error is obtained propagating the errors on events numbers and fractions.

The systematics associated to the observables are reported in Table 4 and they are evaluated in the same way as described in the note for the other observables.

Final results are:

$$\begin{aligned} \mathcal{R}^+_{ADS}(\pi) &= (2.4 \pm 1.0 \pm 0.4) \cdot 10^{-3} \\ \mathcal{R}^-_{ADS}(\pi) &= (3.1 \pm 1.1 \pm 0.4) \cdot 10^{-3} \\ \mathcal{R}^+_{ADS}(K) &= (42.6 \pm 13.7 \pm 2.8) \cdot 10^{-3} \\ \mathcal{R}^-_{ADS}(K) &= (3.8 \pm 10.3 \pm 2.7) \cdot 10^{-3} \end{aligned}$$

$R^+_{ADS}(\pi)$	$R^-_{ADS}(\pi)$	$R_{ADS}(\pi)$ fitted	$R_{ADS}(\pi)$ calculated
0.0024	0.0031	0.0028	0.0028
		$A_{ADS}(\pi)$ fitted	$A_{ADS}(\pi)$ calculated
		0.13	0.13

Table 5: Results comparison between the fitted $R_{ADS}(\pi)$ and $A_{ADS}(\pi)$ and the values calculated from $R^+(\pi)$ and $R^-(\pi)$.

$R^+_{ADS}(K)$	$R^-_{ADS}(K)$	$R_{ADS}(K)$ fitted (uncorrected)	$R_{ADS}(K)$ calculated
0.0426	0.0038	0.0222	0.0232
		$A_{ADS}(K)$ fitted	$A_{ADS}(K)$ calculated
		-0.82	-0.83

Table 6: Results comparison between the fitted $R_{ADS}(K)$ and $A_{ADS}(K)$ and the values calculated from $R^+(K)$ and $R^-(K)$.

In Tables 5 and 6 we reported the results comparison between the fitted R_{ADS} and A_{ADS} and the values calculated from R^+/R^- using the equations (20), for the pion and kaon modes respectively.

We find agreement in the pion's values, but disagreement in the kaon case.

As a comparison, we checked the BaBar results for the $B^- \to DK^-$, $B^- \to D\pi^-$ [18] and $B^- \to [K\pi\pi^0]_D K^-$ [19] (Tables 7, 8 and 9 respectively), finding a disagreement also in their results in the kaon modes.

$R^+_{ADS}(\pi)$	$R^-_{ADS}(\pi)$	$R_{ADS}(\pi)$ fitted	$R_{ADS}(\pi)$ calculated
0.0032	0.0034	0.0033	0.0033
		$A_{ADS}(\pi)$ fitted	$A_{ADS}(\pi)$ calculated
		0.03	0.03

Table 7: BaBar results comparison between the fitted $R_{ADS}(\pi)$ and $A_{ADS}(\pi)$ and the values calculated from $R^+(\pi)$ and $R^-(\pi)$.

$R^+_{ADS}(K)$	$R^-_{ADS}(K)$	$R_{ADS}(K)$ fitted (uncorrected)	$R_{ADS}(K)$ calculated
0.022	0.002	0.011	0.012
		$A_{ADS}(K)$ fitted	$A_{ADS}(K)$ calculated
		-0.86	-0.91

Table 8: BaBar results comparison between the fitted $R_{ADS}(K)$ and $A_{ADS}(K)$ and the values calculated from $R^+(K)$ and $R^-(K)$.

$R^+_{ADS}(K)$	$R^-_{ADS}(K)$	$R_{ADS}(K)$ fitted (uncorrected)	$R_{ADS}(K)$ calculated
0.005	0.012	0.0091	0.0085

Table 9: BaBar results comparison between the fitted $R_{ADS}(K)$ and $A_{ADS}(K)$ and the values calculated from $R^+(K)$ and $R^-(K)$ in the $B^- \to [K\pi\pi^0]_D K^-$ mode.

B $\frac{K^-\pi^+}{K^+\pi^-}$ efficiency

We can evaluate the $K^-\pi^+/K^+\pi^-$ efficiency using our favored sample of $B^- \to D^0\pi^-$ decay, for which we expect zero asymmetry. The pdg value, which accounts only for a Belle result of 2006, is -0.008 ± 0.008 [17], compatible with zero.
On our data we found $N(B^+) = 9881 \pm 103$ and $N(B^-) = 9893 \pm 103$, so the asymmetry of the favored pion mode[5] is equal to $A^m_{fav}(\pi) = (0.6 \pm 7.3) \cdot 10^{-3}$.

To evaluate the efficiency we can in this way.

B.1 Strategy

- The central value of the efficiency is evaluated considering a true value of the asymmetry equal to zero.
- The statistical error is obtained propagating the error on the efficiency of the pion from B and the error on the measured asymmetry.
- The systematic error is obtained propagating the error on the pdg measurement of the asymmetry.

In the following the calculation.

B.2 Calculation

B.2.1 How compare the measured asymmetry with the true asymmetry and the efficiency

The number of measured events (N^m) can be written as $N^t \cdot \epsilon$, where N^t is the true number of events and ϵ is the efficiency of reconstruction.

The true value of the asymmetry is:

$$A^t_{fav}(\pi) = \frac{N([K^-\pi^+]\pi^-) - N([K^+\pi^-]\pi^+)}{N([K^-\pi^+]\pi^-) + N([K^+\pi^-]\pi^+)} = \frac{N^{t-}_f - N^{t+}_f}{N^{t-}_f + N^{t+}_f} = \frac{N^{t-}_f/N^{t+}_f - 1}{N^{t-}_f/N^{t+}_f + 1}$$

from which $N^{t-}_f/N^{t+}_f = \frac{1 + A^t_{fav}}{1 - A^t_{fav}}$.

The total efficiency (ϵ) we are considering is:

$$\epsilon^- = \epsilon(K^-\pi^+) \cdot \epsilon(\pi^-) = \epsilon^-_D \cdot \epsilon^-_\pi$$

$$\epsilon^+ = \epsilon(K^+\pi^-) \cdot \epsilon(\pi^+) = \epsilon^+_D \cdot \epsilon^+_\pi.$$

[5] the asymmetry is calculated using all digits of the numbers of events

so we can write the measured asymmetry:

$$A^m_{fav}(\pi) = \frac{N_f^{m-} - N_f^{m+}}{N_f^{m-} + N_f^{m+}} = \frac{N_f^{t-} \cdot \epsilon^- - N_f^{t+} \cdot \epsilon^+}{N_f^{t-} \cdot \epsilon^- + N_f^{t+} \cdot \epsilon^+} = \frac{N_f^{t-}/N_f^{t+} \cdot \epsilon^-/\epsilon^+ - 1}{N_f^{t-}/N_f^{t+} \cdot \epsilon^-/\epsilon^+ + 1}$$

from which $\epsilon^-/\epsilon^+ = \dfrac{1}{N_f^{t-}/N_f^{t+}} \cdot \dfrac{1+A^m}{1-A^m}$,

$$\frac{\epsilon_D^-}{\epsilon_D^+} \cdot \frac{\epsilon_\pi^-}{\epsilon_\pi^+} = \left(\frac{1-A^t}{1+A^t}\right)\left(\frac{1+A^m}{1-A^m}\right)$$

$$\downarrow$$

$$\frac{\epsilon_D^-}{\epsilon_D^+} = \frac{\epsilon_\pi^+}{\epsilon_\pi^-} \cdot \left(\frac{1-A^t}{1+A^t}\right)\left(\frac{1+A^m}{1-A^m}\right) \tag{21}$$

B.2.2 Efficiency central value

To evaluate the central value we use $A^t = 0$,

$$\frac{\epsilon_D^-}{\epsilon_D^+} = \frac{\epsilon_\pi^+}{\epsilon_\pi^-} \cdot \left(\frac{1+A^m}{1-A^m}\right) \tag{22}$$

and $\epsilon_\pi^+/\epsilon_\pi^- = 0.997 \pm 0.003$ [16]. In this way:

$$\frac{\epsilon_D^-}{\epsilon_D^+} = \frac{\epsilon(K^-\pi^+)}{\epsilon(K^+\pi^-)} = 0.998.$$

B.2.3 Efficiency statistical error

Propagating the error on the pion efficiency and on the measured asymmetry in (22) we obtain this expression:

$$\Delta\frac{\epsilon_D^-}{\epsilon_D^+}(stat) = \sqrt{\left(\frac{1+A^m}{1-A^m}\right)^2 \left(\Delta\epsilon_\pi^-/\epsilon_\pi^+\right)^2 + \left(\frac{2\epsilon_\pi^-/\epsilon_\pi^+}{(1-A^m)^2}\right)^2 (\Delta A^m)^2}.$$

The statistical error is equal to 0.015.

B.2.4 Efficiency systematic error

To evaluate the systematic error we can use the complete formula (21) and propagate the error on the pdg measurement. The formula is:

$$\Delta\frac{\epsilon_D^-}{\epsilon_D^+}(syst) = \left(\frac{1+A^m}{1-A^m}\right) \cdot \frac{2\epsilon_\pi^-/\epsilon_\pi^+}{(1+A^t)^2} \cdot (\Delta A^t)$$

The final result is:

$$\frac{\epsilon_D^-}{\epsilon_D^+} = \frac{\epsilon(K^-\pi^+)}{\epsilon(K^+\pi^-)} = 0.998 \pm 0.015(stat) \pm 0.016(syst).$$

C D^0 BR used in the $B \to [X]_D \pi$ and $B \to [X]_D K$ MC samples.

```
Decay D0
# updated according to suggestions by P. Roudeau,
# using PDG2004 measurements and imposing the equality
# of sl partial widths for D+ and D0.
# Include additional decay anti-K0 pi- e+ nu_e , K- pi0 e+ nu_e.
#
0.0225   K*-  e+  nu_e           PHOTOS   ISGW2;
0.0350   K-   e+  nu_e           PHOTOS   ISGW2;
0.0014   K_1-  e+  nu_e           PHOTOS   ISGW2;
0.0015   K_2*- e+  nu_e           PHOTOS   ISGW2;
0.0034   pi-  e+  nu_e           PHOTOS   ISGW2;
0.0022   rho- e+  nu_e           PHOTOS   ISGW2;
0.0011   anti-K0  pi-  e+  nu_e  PHOTOS   PHSP;
0.0006   K-  pi0  e+  nu_e       PHOTOS   PHSP;
#
0.0214   K*-  mu+ nu_mu          PHOTOS  ISGW2;
0.0340   K-   mu+ nu_mu          PHOTOS  ISGW2;
0.0014   K_1-  mu+ nu_mu          PHOTOS  ISGW2;
0.0015   K_2*- mu+ nu_mu          PHOTOS  ISGW2;
0.0034   pi-  mu+ nu_mu            PHOTOS  ISGW2;
0.0022   rho- mu+ nu_mu            PHOTOS  ISGW2;
0.0011   anti-K0  pi-  mu+  nu_mu  PHOTOS   PHSP;
0.0006   K-  pi0  mu+  nu_mu       PHOTOS   PHSP;
#
0.0383   K-  pi+                          PHSP;
0.0212   anti-K0   pi0                        PHSP;
0.0071   anti-K0   eta                        PHSP;
0.0172   anti-K0   eta'                       PHSP;
0.0210   omega anti-K0                         SVS;
0.0190   anti-K*0 eta                        SVS;
0.0020   anti-K*0 eta'                       SVS;
0.0730   a_1+ K-                           SVS;
0.0610   K*- rho+                          SVV_HELAMP  1.0 0.0 1.0 0.0 1.0 0.0;
0.0146   anti-K*0 rho0                     SVV_HELAMP  1.0 0.0 1.0 0.0 1.0 0.0;
0.0110   anti-K*0 omega                    SVV_HELAMP  1.0 0.0 1.0 0.0 1.0 0.0;
# the Dalitz mode below includes K*bar(892)0 pi0,
# K*(892)- pi+, and K- rho(770)+ resonances
0.1390   K-  pi+  pi0                     D_DALITZ;
0.0085   K*BR pi0                         SVS;
0.0107   K_1- pi+                          SVS;
```

```
0.0071   anti-K_10 pi0                          SVS;
#
# the Dalitz mode below includes K*(892)- pi+ and Kbar0 rho(770)0 resonances
0.0540   anti-K0   pi+  pi-                     D_DALITZ;
0.0078   anti-K0   pi0  pi0                     PHSP;
0.0225   anti-K*0 pi+  pi-                     PHSP;
0.0116   anti-K*0 pi0  pi0                     PHSP;
0.0100   K*- pi+  pi0                    PHSP;
0.0068   K-  rho+ pi0                    PHSP;
0.0060   K-  pi+  rho0                   PHSP;
0.0303   K-  pi+  omega                   PHSP;
0.0100   K-  pi+  eta                    PHSP;
0.0075   K-  pi+  eta'                   PHSP;
0.0074   K-  pi+  pi+   pi-              PHSP;
0.0085   anti-K0   pi+  pi-   pi0              PHSP;
#
# K- pi+ pi0 pi0 is (15 +/- 5)\% in the PDG, but we decrease it to
# have everything add to 1 and get enough neutral kaons:
0.02575  K-  pi+  pi0   pi0              PHSP;
#
0.0143   anti-K0   pi0  pi0   pi0              PHSP;
0.0038   K-  pi+  pi+   pi-   pi0        PHSP;
0.0038   K-  pi+  pi0   pi0   pi0        PHSP;
0.0058   anti-K0   pi+  pi-   pi+   pi-        PHSP;
#
0.0638   anti-K0   pi+  pi-   pi0   pi0        PHSP;
0.0192   anti-K0   pi+  pi-   pi0   pi0   pi0  PHSP;
#
0.0086   phi anti-K0                           SVS;
0.0051   anti-K0   K+   K-                     PHSP;
0.0008   K_S0 K_S0  K_S0                   PHSP;
0.0043   K+  K-                          PHSP;
0.0006   K_S0 K_S0                         PHSP;
0.0006   K_L0 K_L0                         PHSP;
0.0004   K*0 anti-K0                           SVS;
0.0008   anti-K*0 K0                         SVS;
0.0018   K*- K+                          SVS;
0.0035   K*+ K-                          SVS;
0.0014   anti-K*0 K*0                         SVV_HELAMP 1.0 0.0 1.0 0.0 1.0 0.0;
0.0007   phi pi0                          SVS;
0.0011   phi pi+  pi-                    PHSP;
0.0025   K+  K-   pi+  pi-               PHSP;
0.0030   K+  K-   pi0  pi0               PHSP;
0.0015   anti-K0   K0   pi+  pi-              PHSP;
```

```
0.0015   anti-K0   K0   pi0  pi0              PHSP;
#
0.0015   pi+ pi-                          PHSP;
0.0008   pi0 pi0                          PHSP;
0.0010   eta pi0                          PHSP;
0.0010   eta'  pi0                        PHSP;
0.0010   eta eta                          PHSP;
0.0040   rho+ pi-                         SVS;
0.0040   rho- pi+                         SVS;
0.0020   rho0 pi0                         SVS;
0.0060   pi+  pi-  pi0                    PHSP;
0.0010   pi0  pi0  pi0                    PHSP;
0.0073   pi+  pi+  pi-  pi-               PHSP;
0.0050   pi+  pi-  pi0  pi0               PHSP;
0.0177   pi+  pi-  pi+  pi-  pi0          PHSP;
0.0060   pi+  pi-  pi0  pi0  pi0          PHSP;
#
# Doubly Cabibbo suppressed decays:
0.00015   pi-  K+                          PHSP;
0.0005    pi-  K+  pi0                     PHSP;
Enddecay
#
#
```

References

[1] D. Atwood, I. Dunietz, A. Soni, "Enhanced CP violation with $B \to D(\bar{D})$ modes and extraction of the Cabibbo-Kobayashi-Maskawa angle γ.", Phys. Rev. Lett. 78, 3257, (1997).

[2] D. Atwood, I. Dunietz, A. Soni, "Improved methods for observing CP violation with $B^{\pm} \to KD$ and measuring the CKM phase γ.", Phys. Rev. D 63, 036005, (2001).

[3] M.Gronau, D.Wyler, PLB 265,172.

[4] M.Gronau, D.London, PLB 253,483.

[5] A.Giri, Y.Grossman, A.Soffer, J.Zupan, PRD 68, 054018.

[6] The Heavy Flavor Averaging Group. http://www.slac.stanford.edu/xorg/hfag/index.html

[7] CKMfitter Group (J. Charles et al.), Eur. Phys. J. C41, 1-131 (2005), [hep-ph/0406184], updated results and plots available at: http://ckmfitter.in2p3.fr.

[8] P.Squillacioti et al., "Measurements of branching fractions and CP asymmetries in $B+ \to DcpK+$", CDF-note 8993.

[9] CDF Colaboration, "Measurements of branching fraction ratios and CP asymmetries in $B^{\pm} \to D_{CP}K^{\pm}$ decays in hadron collisions", Phys.Rev.D81:031105,2010.

[10] G. Punzi, *"Sensitivity of searches for new signals and its optimization."*, arXiv:0308063v2 [physics.data-an], (2003).

[11] P. Squillacioti et al., "Update of Combined PID in 5.3.4" CDF-note 7866.

[12] P. Squillacioti et al., "Update of Combined PID in 6.1.4" CDF-note 8478.

[13] http://www-cdf.fnal.gov/internal/physics/bottom/bpak/pid/CombPID_page.html

[14] G. Cowan, " Statistical data analysis", Oxford Science Publications, 1998.

[15] http://www-cdf.fnal.gov/htbin/twiki/bin/view/TOFandDeDx/DeDxCalibration

[16] S. Giagu et al., "Relative Branching Fractions and CP-violating decay rate Asymmetries in Cabibbo suppressed decays of the D^0 meson" CDF-note 6391.

[17] K. Nakamura et al. (Particle Data Group), J. Phys. G 37, 075021 (2010).

[18] P. del Amo Sanchez et al. (The BABAR Collaboration), *"Search for $b \to u$ transitions in $B^- \to DK^-$ and D^*K^- decays"*, Phys. Rev. D 82, 072006 (2010).

[19] J.-P. Lees, et al (The BABAR Collaboration), *"Search for $b \to u$ transitions in $B^- \to [K^+\pi^-\pi^0]_D K^-$ decays"*, arXiv:1104.4472v1 [hep-ex].